Parton distributions of the proton

A. D. Martin and W. J. Stirling
Department of Physics, University of Durham, Durham DH1 3LE, England

R. G. Roberts
Rutherford Appleton Laboratory, Chilton, Didcot OX11 0QX, England
(Received 8 June 1994)

To obtain improved parton densities of the proton, we present a new global analysis of deep-inelastic and related data including, in particular, the recent measurements of F_2 at DESY HERA, of the asymmetry of the rapidity distributions of $W^{\pm}$ production at the Fermilab $p\bar{p}$ collider and of the asymmetry in Drell-Yan production in pp and pn collisions. We also incorporate data to determine the flavor dependence of the quark sea distributions. We find that the behavior of the partons at small x is consistent with the precocious onset of BFKL leading $\ln(1/x)$ dynamics. We discuss the ambiguities remaining in the gluon distribution. We present improved predictions for W boson (and t quark) production at the Fermilab $p\bar{p}$ collider.

PACS number(s): 13.60.Hb, 12.38.Bx, 12.38.Qk, 13.15.+g

I. INTRODUCTION

The increased precision in the experimental measurements of deep-inelastic scattering and related processes over the last few years has led to a considerable improvement in our knowledge of the parton distributions of the proton. However, several significant sets of measurements have become available since the last global analyses of the data were performed to determine the parton densities. The new data may be divided into two groups. First, we have the measurements of the structure function $F_2(x,Q^2)$ for electron-proton deep-inelastic scattering for $x \lesssim 10^{-3}$ by the H1 and ZEUS Collaborations at the DESY ep collider HERA [1–3], and second, the measurement of the asymmetry in Drell-Yan production in pp and pn collisions by the NA51 Collaboration at CERN [4] and of the asymmetry of the $W^{\pm}$ rapidity distributions by the Collider Detector at Fermilab (CDF) Collaboration [5]. The two groups of measurements have quite distinct implications for the partons and are, therefore, to a great extent decoupled. The HERA F_2 data offer the first constraints on partons in the previously unexplored small-x regime, whereas the two asymmetry measurements probe fine details of the quark distributions in the region $x \sim 0.1$. The latter information is crucial, for example, for a precise determination of the mass of the W boson at the Fermilab collider.

Figure 1 shows the dramatic rise of F_2 with decreasing x, which was first observed by the H1 and ZEUS Collaborations [1]. Also shown are the extrapolated predictions for F_2 at Q^2=15 GeV^2 from two parton sets (D'_0,D'_-) [8] made before the HERA measurements became available, but which it was believed would span the data. The upper limit, the curve D'_-, was motivated by assuming the precocious onset of Balitsky-Fadin-Kuraev-Lipatov (BFKL) dynamics [9] in which the gluon and sea quark distributions have the singular form

$$xg, xq_{\rm sea} \sim x^{-0.5} \tag{1}$$

as $x \to 0$, whereas the D'_0 curve was the lower limit anticipated from conventional Regge expectations with

$$xg, xq_{\rm sea} \sim x^{0} \ . \tag{2}$$

Such extrapolations are notoriously unreliable and have failed in the past. Moreover, as we will see in Sec. III, the connection with precocious BFKL behavior turns out to be more subtle than (1) would suggest. Although D'_0 and D'_- are the most recent published Martin-Roberts-

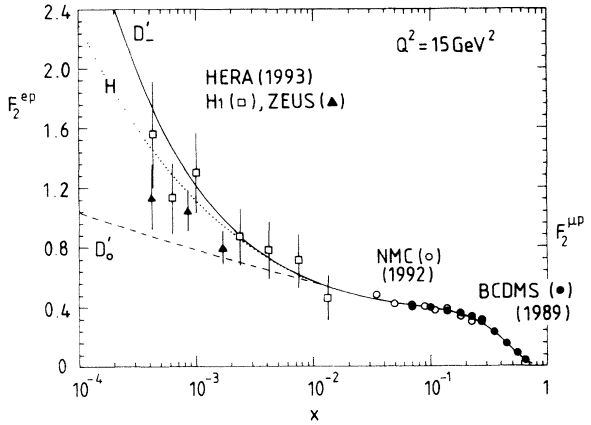

FIG. 1. H1 and ZEUS data [1] obtained from the 1992 HERA run, but published in 1993, together with earlier data (interpolated to Q^2=15 GeV^2) obtained by the NMC [6] and BCDMS Collaborations [7]. The "pre-HERA" extrapolations obtained using MRS(D'_0,D'_-) parton sets [8] were expected to span the forthcoming HERA measurements. The "post-HERA" curve H is the result of a global analysis [10] which included the HERA data.

Stirling (MRS) sets of partons, a set MRS(H) was subsequently made available,[1] which was obtained from a global analysis that incorporated the measurements [1] of F_2 from the 1992 HERA run. The curve denoted by H in Fig. 1 is an example of the quality of the fit. The main feature is that the HERA measurements required a small-x behavior of the form

$$xg, xq_{\rm sea} \sim x^{-0.3} \ . \tag{3}$$

Higher statistics measurements of F_2, obtained from the 1993 HERA run, have just become available in preliminary form [2,3]. We incorporate these data in our new global analysis and in Sec. III we discuss the implications for the small-x behavior of the partons and for QCD dynamics. The new HERA data for F_2 are in line with the old (i.e., show the same rise with decreasing x), and in fact the MRS(H) partons still give an excellent fit in the HERA small-x region.

The data in Figs. 2 and 3 are, respectively, the measurement of the asymmetry in Drell-Yan production in pp and pn collisions [4],

$$A_{\rm DY} = \frac{\sigma_{pp} - \sigma_{pn}}{\sigma_{pp} + \sigma_{pn}} \ , \tag{4}$$

and of the asymmetry of the rapidity distributions of the charged leptons from $W^{\pm} \to l^{\pm}\nu$ decays at Fermilab [5]:

$$A(y_l) = \frac{\sigma(l^+) - \sigma(l^-)}{\sigma(l^+) + \sigma(l^-)} \ . \tag{5}$$

In (4), $\sigma \equiv d^2\sigma/dM\,dy|_{y=0}$, where M and y are the invariant mass and rapidity of the produced lepton pair, while, in (5), $\sigma(l^{\pm}) \equiv d\sigma/dy_l$ are the differential $p\bar{p} \to W^{\pm}X \to l^{\pm}\nu X$ cross sections for producing $l^{\pm}$ leptons of rapidity y_l. Also shown are the predictions of MRS(H) and the equivalent set of partons, CTEQ2M, obtained by the CTEQ Collaboration [11]. We see that neither set of partons gives a satisfactory description of both asymmetries. This deficiency of the parton sets is not surprising. The reason is that the high-precision muon and neutrino deep-inelastic structure function data, which provide the core constraints of the global analyses, do not pin down the combination $\bar{d} - \bar{u}$ of parton densities. Indeed, the Drell-Yan asymmetry experiment was proposed [12] as it was uniquely equipped to determine just this combination of densities. The asymmetry data therefore offer a fine-tuning of the u, d, $\bar{u}$, and $\bar{d}$ parton densities in the region $x \sim 0.1$, which is invaluable for the precision studies of the W boson at Fermilab. To this end we include for the first time the asymmetry data in the global analysis (together with the new HERA measurements of F_2) and find a new set of partons, which we denote MRS(A). The resulting description of the asymmetry measurements is also shown in Figs. 2 and 3. We discuss this aspect of the global analysis in Sec. IV.

[1] A brief description of MRS(H) can be found in Ref. [10].

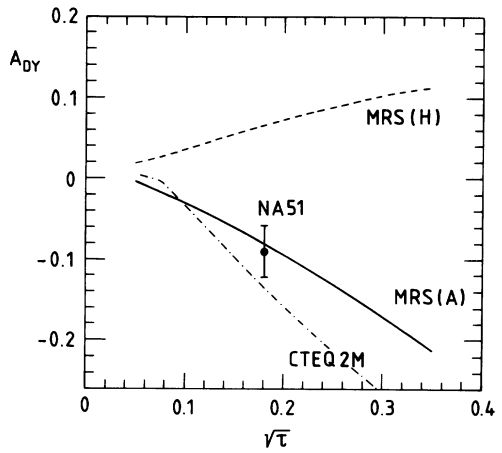

FIG. 2. Measurement of the asymmetry in Drell-Yan production in pp and pn collisions made by the NA51 Collaboration [4] at $x = \sqrt{\tau}$=0.18. The curves obtained from MRS(H) [10] and CTEQ2M [11] partons predate the measurement. The MRS(A) curve is obtained from the global fit, presented in this paper, which includes the NA51 data point.

The outline of the paper is as follows. We first explain, in Sec. II, the procedure that we follow to determine the parton densities from a global analysis of the data. We give details of the new improved MRS(A) parton distributions, and we compare them with the MRS(H) set. Sections III and IV consider the impact of the new small-x and asymmetry data, respectively. In Sec. V we discuss the ambiguities in the present knowledge of the gluon. In Sec. VI we update the predictions for W boson and top quark production at the Fermilab $p\bar{p}$ collider, and finally in Sec. VII we present our conclusions.

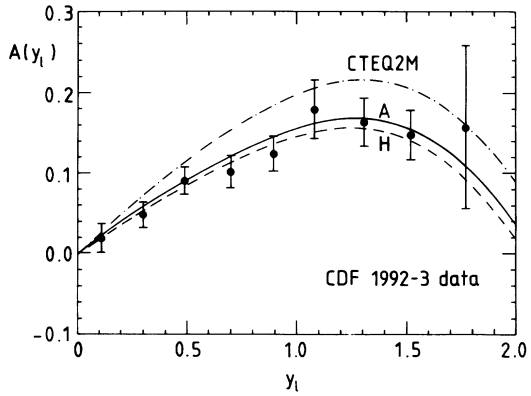

FIG. 3. Asymmetry $A(y_l)$ of the rapidity distributions of the charged leptons from $W^{\pm} \to l^{\pm}\nu$ decays observed at Fermilab [5] as a function of the lepton rapidity y_l. The curves are the next-to-leading-order descriptions obtained using MRS(H) [10], CTEQ2M [11], and the new MRS(A) partons. The MRS(A) analysis, presented in this paper, includes the data in the global fit.

II. GLOBAL ANALYSIS

The parton distributions f_i are determined from a global fit to a wide range of deep-inelastic and related data. The basic procedure is to parametrize the f_i at a sufficiently large Q_0^2 ($Q_0^2 = 4$ GeV^2) so that $f_i(x,Q^2)$ can be calculated at higher Q^2 in perturbative QCD using next-to-leading-order Altarelli-Parisi [Gribov-Lipatov-Altarelli-Parisi (GLAP)] evolution equations. In view of the quantity and variety of data that are fitted, it is remarkable that an excellent description can be obtained with the simple parametrization

$$\begin{aligned} xu_v &= A_u x^{\eta_1}(1-x)^{\eta_2}(1+\epsilon_u\sqrt{x}+\gamma_u x)\ , \\ xd_v &= A_d x^{\eta_3}(1-x)^{\eta_4}(1+\epsilon_d\sqrt{x}+\gamma_d x)\ , \\ xS &= A_S x^{-\lambda}(1-x)^{\eta_S}(1+\epsilon_S\sqrt{x}+\gamma_S x)\ , \\ xg &= A_g x^{-\lambda}(1-x)^{\eta_g}(1+\gamma_g x)\ , \end{aligned} \tag{6}$$

where the valence distributions $u_v \equiv u-\bar{u}$ and $d_v \equiv d-\bar{d}$, and where the total sea distribution $S \equiv 2(\bar{u}+\bar{d}+\bar{s}+\bar{c})$. We assume that $s=\bar{s}$. At present there are not enough experimental constraints on the gluon to justify the introduction of an extra parameter ϵ_g in xg or to determine the exponent λ independent of that of the sea-quark distribution S. Three of the four A_i coefficients are determined by the momentum and flavor sum rules. The distributions are defined in the modified minimal subtraction ($\overline{\rm MS}$) renormalization and factorization scheme, and the QCD scale parameter $\Lambda_{\overline{\rm MS}}(n_f=4)$ is taken as a free parameter.

The flavor structure of the quark sea is taken to be

$$\begin{aligned} 2\bar{u} &= 0.4(1-\delta)S-\Delta\ , \\ 2\bar{d} &= 0.4(1-\delta)S+\Delta\ , \\ 2\bar{s} &= 0.2(1-\delta)S\ , \\ 2\bar{c} &= \delta S\ , \end{aligned} \tag{7}$$

at $Q^2 = Q_0^2 = 4$ GeV^2, with

$$x\Delta \equiv x(\bar{d}-\bar{u}) = A_\Delta x^{\eta_\Delta}(1-x)^{\eta_S}(1+\gamma_\Delta x)\ . \tag{8}$$

The first hint that the u,d flavor symmetry of the sea is broken (with $\bar{d}>\bar{u}$ on average) came from the evaluation of the Gottfried sum by the New Muon Collaboration (NMC) [13]. In fact, until then all global analyses had assumed $\bar{u}=\bar{d}$. As we shall see in Sec. IV, the observed Drell-Yan asymmetry provides further evidence that $\bar{d}>\bar{u}$, which we allow through the parametrization of Δ given in (8). The flavor breaking can be associated with the breaking of $\rho-a_2$ meson Regge exchange degeneracy, and so we choose the exponent η_Δ in (8) to be close to that of the valence quark densities. To be precise, we set η_Δ=0.4 [whereas for MRS(H) we set $\eta_\Delta=\eta_1$=0.335].

As in earlier MRS parametrizations, we assume that the input strange sea is suppressed by 50% in relation to the u and d sea distributions—hence we get the factors of 0.4, 0.4, and 0.2 in Eq. (7). The first indications for such a suppression came from early deep-inelastic dimuon production data, but now there is much firmer evidence for our input assumption. The Chicago-Columbia-Fermilab-Rochester (CCFR) Collaboration [14] have performed a next-to-leading-order analysis of their $\nu N \to \mu^-\mu^+ X$ data and deduce that the strange sea distributions should lie within the shaded band shown in Fig. 4. The strange sea that we find is shown by the curve denoted by MRS(A) in Fig. 4 and satisfies the experimental constraint.

The input charm sea is determined by the European Muon Collaboration (EMC) deep-inelastic data for the structure function F_2^c. We proceed as follows. We assume that

$$c(x,Q^2) = 0 \quad \text{for } Q^2 < m_c^2 \tag{9}$$

and generate a nonzero distribution at higher Q^2 by massless GLAP evolution at next-to-leading order. The structure functions are also calculated using massless coefficient functions. Since $Q^2=m_c^2$ falls below our input scale Q_0^2=4 GeV^2, we use an approximate set of partons to evolve between m_c^2 and 4 GeV^2. Taking zero charm at $Q^2=m_c^2$, we find that the shape of the resulting charm distribution generated at Q^2=4 GeV^2 is well described by the input parametrization of the overall S distribution. As might be expected, the normalization, specified by the parameter δ of (7), depends sensitively on the value chosen for m_c. We adjust δ to give a good description of the F_2^c data for $Q \geq 5$ GeV^2. The fit is shown in Fig. 5 and corresponds to δ=0.02 and to a charm distribution which can be evolved from zero at $Q^2=m_c^2$=2.7 GeV^2. The value δ=0.02 implies that, at the input scale Q_0^2=4 GeV^2, the charm sea carries 0.4% of the proton's momentum, as compared to nearly 4% carried by the strange quark sea.

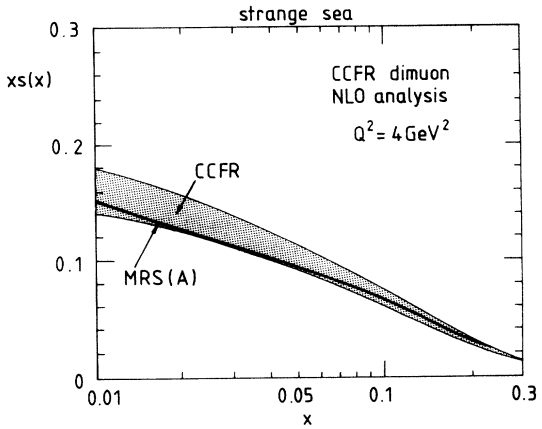

FIG. 4. The shaded band is the strange sea quark distribution xs (x,Q^2=4 GeV^2), determined by the CCFR Collaboration [14] from a next-to-leading-order analysis of their dimuon production data. In addition, they find that $s/(\bar{u}+\bar{d})$ is, to a good approximation, independent of x. Also shown is the MRS(A) input strange sea quark distribution xs ($x,Q_0^2=4$ GeV^2), as given in Eq. (7).

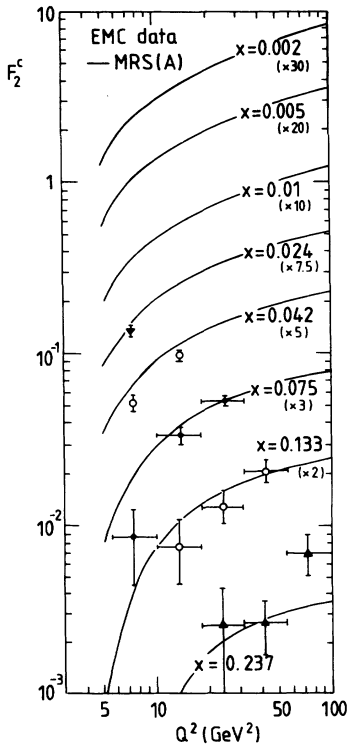

FIG. 5. Description of the EMC data [17] for F_2^c by the MRS(A) partons. We assume that the $c \to \mu + X$ branching ratio is 8%.

Our prescription for the charm quark distributions is only valid far above threshold, $W^2 = Q^2(1-x)/x \gg 4m_c^2$. Near threshold, a more rigorous treatment of quark mass effects is required. As discussed in detail in Ref. [15] (see also [16]), various prescriptions are possible. For example, one can *define* heavy quark densities according to our prescription and absorb the threshold effects into the coefficient functions. Nevertheless, Fig. 5 shows that our treatment of the charm distribution does give a reasonable description of the EMC data [17] for F_2^c with $Q^2 > 5$ GeV^2. These data do in fact lie in the region $W^2 \gg 4m_c^2$. It is interesting to note that our satisfactory description means that these EMC data show no necessity for a small "intrinsic" or nonperturbative charm component, as advocated by Brodsky *et al.* [18], except possibly for one data point at x=0.42 (not shown), which lies well above our fit. Also shown in Fig. 5 are the predictions in the small-x region which are relevant for future measurements at HERA. Note that small x implies large W^2, and so our treatment should be reliable in this region.

It has been argued [19] that the strange sea as measured in neutrino scattering should be different from that in muon scattering on account of the different mass thresholds in $W^*g \to s\bar{c}$ as compared to $\gamma^*g \to s\bar{s}$. In practice, the neutrino data have been corrected by the CCFR Collaboration to approximately take into account the $m_c \neq 0$ effects and to allow for this difference. Our strange and charm seas should be interpreted as those for muon data. Our treatment of the charm sea at large x and modest Q^2 is suspect, but then its contribution is too small to distort the analysis. Finally, the b-quark contribution is included by assuming that

$$b(x, Q^2) = 0 \quad \text{for } Q^2 < m_b^2 \,, \tag{10}$$

with m_b^2=30 GeV^2, and nonzero contributions at higher Q^2 generated by the same "massless" prescription that was used for $c(x, Q^2)$.

The experimental data that are used to constrain the parton densities are listed in Table I, together with the leading-order partonic subprocesses, which helps us to see which features of the distributions are constrained by the various data sets. As far as the global analysis is concerned, the "core" deep-inelastic data for $x \gtrsim 0.01$ are the Bologna-CERN-Dubna-Munich-Saclay (BCDMS) [7]

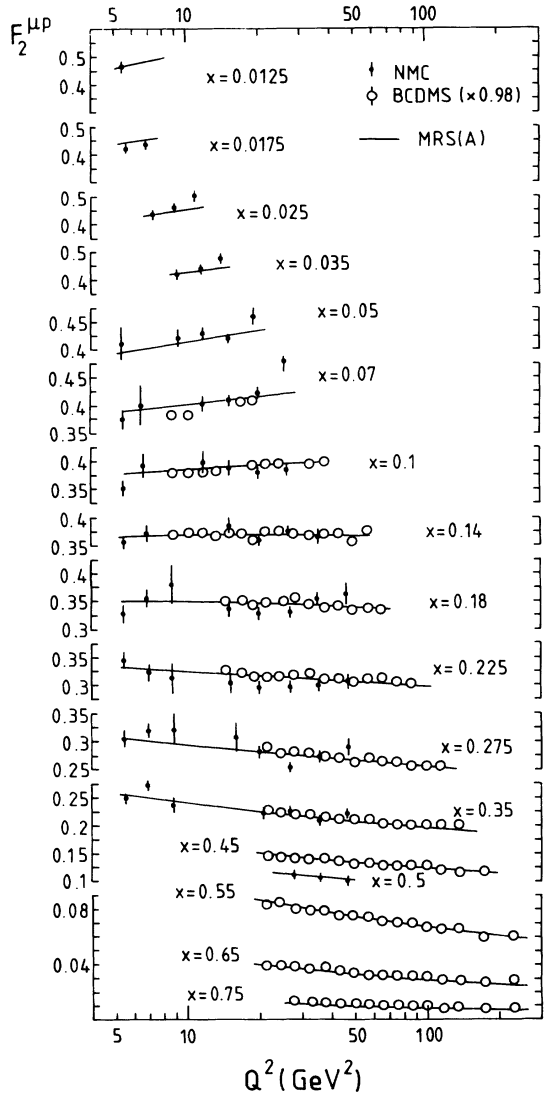

FIG. 6. Description of the BCDMS [7] and NMC [6] measurements of the $F_2^{\mu p}(x, Q^2)$ structure function by the MRS(A) set of partons. The BCDMS data are shown with an overall renormalization by a factor of 0.98.

TABLE I. Experimental data used to determine the MRS parton distributions. The last column gives an indication of the main type of constraint imposed by a particular set of data.

Process/experiment	Leading-order subprocess	Parton determination
DIS ($\mu N \to \mu X$)	$\gamma^* q \to q$	Four structure functions→
BCDMS, NMC		$u + \bar{u}$
$F_2^{\mu p}, F_2^{\mu n}$		$d + \bar{d}$
		$\bar{u} + \bar{d}$
DIS ($\nu N \to \mu X$)	$W^* q \to q'$	s (assumed=$\bar{s}$),
CCFR (CDHSW)		but only $\int xg(x)dx \simeq 0.5$
$F_2^{\nu N}, xF_3^{\nu N}$		$[\bar{u} - \bar{d}$ is not determined]
$\mu N \to c\bar{c}X$	$\gamma^* c \to c$	$c \approx 0.1s$ at Q_0^2
F_2^c, EMC		
$\nu N \to \mu^+\mu^- X$	$W^* s \to c$	$s \approx \frac{1}{2}\bar{u}$ (or $\frac{1}{2}\bar{d}$)
CCFR	$\hookrightarrow \mu^+$	
DIS (HERA)	$\gamma^* q \to q$	λ
F_2^{ep} (H1,ZEUS)		$(x\bar{q} \sim xg \sim x^{-\lambda}$, via $g \to q\bar{q})$
$pp \to \gamma X$	$qg \to \gamma q$	$g(x \approx 0.4)$
WA70 (UA6)		
$pN \to \mu^+\mu^- X$	$q\bar{q} \to \gamma^*$	$\bar{q} = \cdots (1-x)^{\eta_S}$
E605		
$pp, pn \to \mu^+\mu^- X$	$u\bar{u}, d\bar{d} \to \gamma^*$	$(\bar{u} - \bar{d})$ at x=0.18
NA51	$u\bar{d}, d\bar{u} \to \gamma^*$	
$p\bar{p} \to WX(ZX)$	$ud \to W$	u, d at $x_1 x_2 s \simeq M_W^2 \to$
UA2, CDF, D0		$x \approx 0.13$ CERN
		$x \approx 0.05$ Fermilab
$\to W^{\pm}$ asym		slope of u/d at $x \approx 0.05$
CDF		

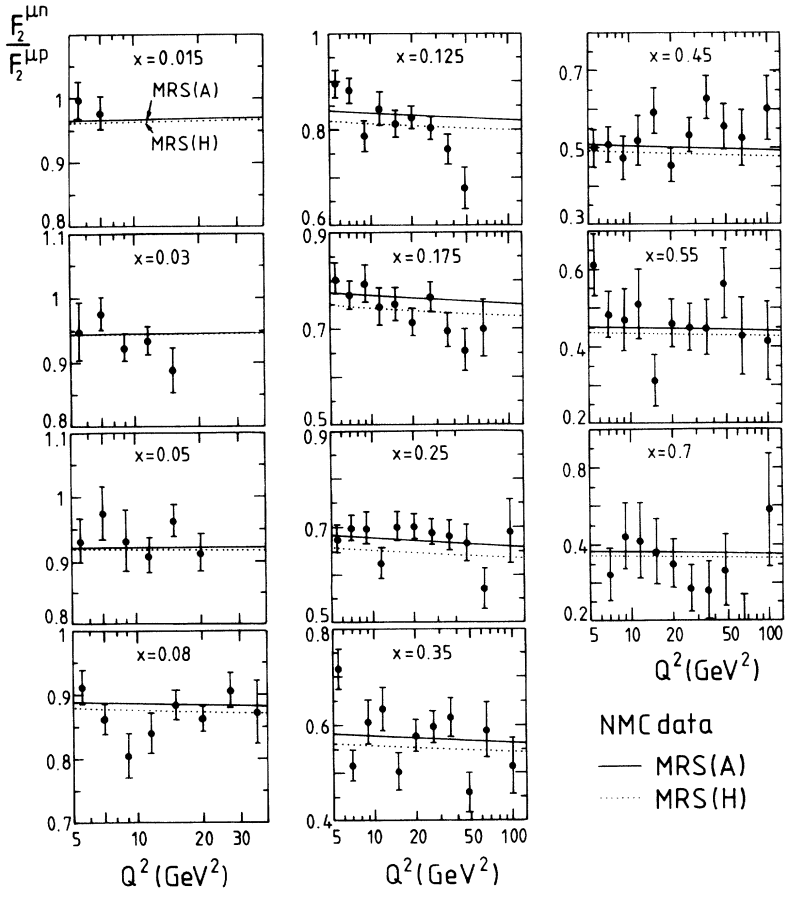

FIG. 7. The solid curves show the description of the NMC data [21] for the structure function ratio $F_2^{\mu n}/F_2^{\mu p}$ given by the MRS(A) set of partons. The data are shown after correction for the effects of deuteron shadowing. We use the corrections calculated by Badelek and Kwieciński [23]. The dotted curves are the predictions of the MRS(H) partons obtained from a global analysis which included an earlier set of NMC data for $F_2^{\mu n}/F_2^{\mu p}$.

and NMC [6,21] measurements of $F_2^{\mu p}$ and $F_2^{\mu n}$ and the CCFR measurements [22] of $F_2^{\nu N}$ and $xF_3^{\nu N}$. It is useful to inspect the leading-order expressions of these structure functions in terms of the quark densities

$$F_2^{\mu p} - F_2^{\mu n} = \tfrac{1}{3}x(u + \bar{u} - d - \bar{d}) \,, \tag{11}$$

$$\tfrac{1}{2}(F_2^{\mu p} + F_2^{\mu n}) = \tfrac{5}{18}x(u + \bar{u} + d + \bar{d} + \tfrac{4}{5}s) \,, \tag{12}$$

$$F_2^{\nu N} = F_2^{\bar{\nu} N} = x(u + \bar{u} + d + \bar{d} + 2s) \,, \tag{13}$$

$$\tfrac{1}{2}x(F_3^{\nu N} + F_3^{\bar{\nu} N}) = x(u - \bar{u} + d - \bar{d}) \,, \tag{14}$$

where N is an isoscalar nuclear target and where, for simplicity, we have neglected the small c-quark contribution. On a (x, Q^2) point-by-point basis, these four observables determine four combinations of quark densities, which we may take to be $u + \bar{u}$, $d + \bar{d}$, $\bar{u} + \bar{d}$, and s. The difference $\bar{d} - \bar{u}$ is not determined, and moreover, at leading-order it appears that the only constraint on the gluon is through the momentum sum rule.

From (11) and (12) we see that the strange quark distribution is essentially determined by the structure function difference

$$xs(x) \simeq \tfrac{5}{6}F_2^{\nu N}(x) - 3F_2^{\mu D}(x) \,. \tag{15}$$

At small $x \lesssim 0.08$ the value obtained is significantly larger than that found in the dimuon analyses that we mentioned above. We believe the dimuon result is more reliable, as the determination based on (15) is very sensitive to the relative normalization of two different data sets and to the heavy target corrections that have to be applied to the neutrino data. However, it does mean that in the global analysis this discrepancy will show up in the description of $F_2^{\nu N}$ and/or $F_2^{\mu D}$ at small x. The quality of the MRS(A) fit to the deep-inelastic data is shown in Figs. 6–8. We note that the discrepancy occurs in the description of $F_2^{\nu N}$ at $x \lesssim 0.05$ [see Fig. 8(a)]. We allow an overall normalization parameter for the CCFR data. When we fit to all data (satisfying our $Q^2 > 5$ GeV^2, $W^2 > 10$ GeV^2 criteria), we find a normalization factor

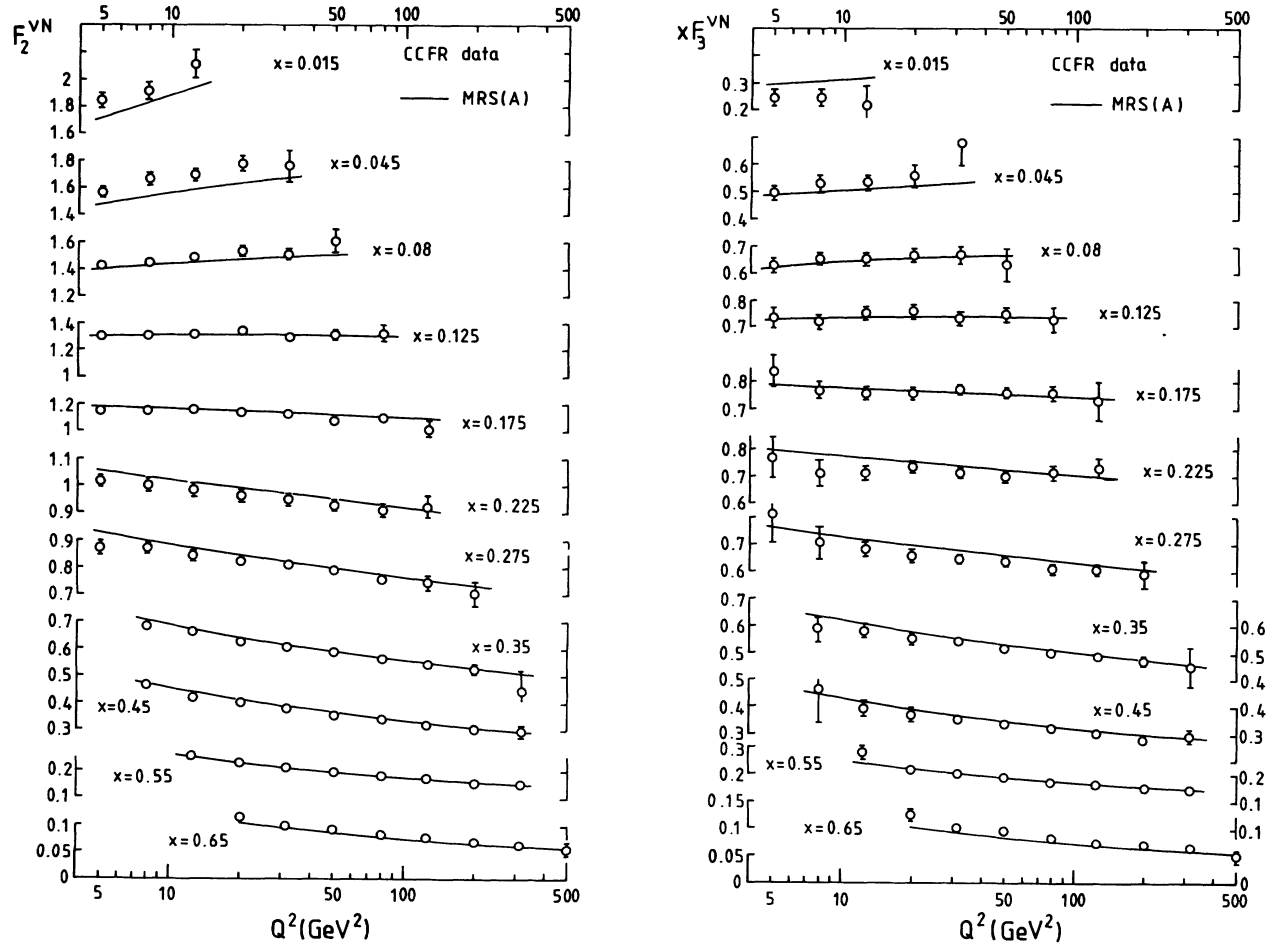

FIG. 8. MRS(A) fit to the CCFR measurements [22] of the structure functions $F_2^{\nu N}$ and $xF_3^{\nu N}$. The data are shown after correction for the heavy target effects and after an overall renormalization of 0.95 required by the global analysis, see text. The statistical, systematic, and heavy target correction errors have been combined in quadrature (see also Ref. [8]).

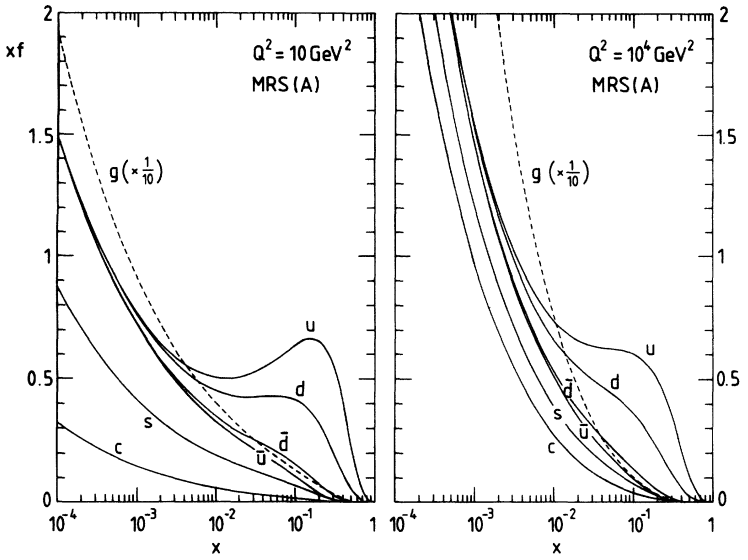

FIG. 9. MRS(A) partons shown as a function of x at $Q^2 = 10$ and 10^4 GeV^2.

of 0.95. If, however, we were to exclude the $x \leq 0.08$ CCFR data, then the normalization factor becomes 0.97 and the description of the remaining neutrino data improves (χ^2 =90 for 132 data points as compared to 171 for 160 points).

Heavy nuclear target corrections are applied to the neutrino data, and deuteron screening corrections are made to the small-x muon-deuterium data as described in Ref. [20]. As in the earlier analyses [20,8,10], the WA70 prompt photon data[2] [24] and the E605 Drell-Yan production data [25] are included in the fit. The former constrain the gluon, and the latter pin down the shape of the sea quark distributions.

The values of the parameters of the starting distributions [Eqs. (6)] of the new MRS(A) set of partons are listed in Table II. In addition, the value of the QCD scale parameter is found to be $\Lambda_{\overline{\rm MS}}(n_f = 4)$=230 MeV, which corresponds to $\alpha_s(M_Z^2)$=0.112$_5$, as was for the MRS(H) set of partons. The parameter values for this latter set are also listed in Table II.[3] Figure 9 shows the MRS(A) parton distributions as a function of x for two different values of Q^2. A comparison of the "new" MRS(A) and "old" MRS(H) parton is shown when we discuss the fit to the Drell-Yan asymmetry measurement in Sec. IV A, since the differences between the two sets arise mainly from introducing this data point into the global analysis. Finally, we show in Table III how the proton's momentum is shared among the various parton flavors in the new MRS(A) set at different Q^2 values.

[2]See Sec. V for a discussion of other prompt photon data.

[3]For MRS(H) and previous MRS analyses, we parametrized $x(u_v + d_v)$ by the expression that we use here for xu_v. Thus parameters marked with a dagger in Table II correspond to $x(u_v + d_v)$ and not to xu_v. To improve the precision at small x, we have repeated the MRS(H) analysis, and so the MRS(H) parameters listed in the table are not precisely the same as those of Ref. [10].

III. SMALL-x BEHAVIOR

The new measurements of F_2^{ep} obtained by the ZEUS [3] and H1 [2] Collaborations in the low-x regime, $x \lesssim 0.005$, are shown in Figs. 10 and 11. These data were included in the global analysis and are, in fact, the only constraint on the parameter λ in (6) which controls the small-x behavior of the sea $xS \sim x^{-\lambda}$ (and of the gluon $xg \sim x^{-\lambda}$). The existing set of partons, MRS(H) with λ=0.3, is found to give an excellent description of the new data, and so it is not surprising that the new parametrization MRS(A) has the same value of λ. The

TABLE II. Numerical values of the starting distributions (6) of the MRS(A) set of partons. For comparison, we also list the values corresponding to the MRS(H) partons. Note that A_g is fixed by the momentum sum rule and is therefore not a free parameter. The parameters marked with a dagger correspond to $x(u_v + d_v)$ and not to xu_v (see footnote 3).

		MRS(A)	MRS(H)
Glue	(A_g)	0.775	0.777
	λ	0.3	0.3
	η_g	5.3	5.3
	γ_g	5.2	5.2
Valence	η_1	0.538	0.335†
	η_2	3.96	3.90†
	ϵ_u	−0.39	4.40†
	γ_u	5.13	8.95†
	η_3	0.330	0.224
	η_4	4.71	4.65
	ϵ_d	5.03	44.3
	γ_d	5.56	13.2
Sea	A_S	0.411	0.386
	η_S	9.27	9.01
	ϵ_S	−1.15	0.11
	γ_S	15.6	12.6
	A_Δ	0.099	0.055
	γ_Δ	25.0	

TABLE III. Fractions (in percent) of the total proton momentum carried by the various partons in the MRS(A) set.

Q^2 (GeV^2)	g	u_v	d_v	$2\bar{u}$	$2\bar{d}$	$2s$	$2c$	$2b$
4	42.9	28.5	10.2	5.9	8.5	3.6	0.4	
20	44.8	25.1	9.1	6.3	8.6	4.2	1.4	
100	46.0	22.9	8.2	6.5	8.6	4.7	2.0	0.7
10^4	48.0	18.8	6.8	7.0	8.7	5.5	3.3	2.2

description of the HERA data is shown in Figs. 10 and 11, together with that of the extrapolations obtained from the pre-HERA MRS (D_0',D_-') parton sets.

A. Predictions from perturbative QCD

The value of λ is of great importance for understanding QCD dynamics in the small-x regime. Therefore, before we discuss the uncertainty and the implications of the λ=0.3 determination, it is useful to briefly review the perturbative QCD expectations for the small-x behavior of F_2. In the small-x regime, we encounter large $\ln(1/x)$ contributions which have to be resummed. It is necessary to distinguish two different limits: first, the BFKL limit of small x and moderate $Q^2 \gtrsim Q_0^2$ in which we sum the large $\ln(1/x)$ terms, but keep the full Q^2 dependence, not just the leading-lnQ^2 contributions; second, the small-x and large-Q^2/Q_0^2 region where the double-leading-logarithm approximation of GLAP evolution is appropriate, in which the $\alpha_s \ln(1/x)\ln(Q^2/Q_0^2)$ contributions are resummed. Ideally, we seek a formalism which embodies both limits. Some progress has been made by Marchesini *et al.* [26] to find a unified evolution equation, but much remains to be done before we can extract the form of the small-x behavior of partons. However, we explain below why this is not a serious obstacle to the extraction of partons from the small-x HERA data.

First, we review the BFKL expectations at small x. The BFKL equation is effectively the leading-$\alpha_s \ln(1/x)$ resummation of soft gluon emissions. The equation may be solved numerically and the k_T-factorization theorem used to predict the small-x behavior of F_2. It is found [27] that

$$F_2(x,Q^2) = C(x,Q^2)x^{-\lambda_L} + F_2^{\rm bg}(x,Q^2)\ , \qquad (16)$$

where the coefficient C of the BFKL contribution and the non-BFKL term, $F_2^{\rm bg}$ are weakly dependent on x. The *magnitude* of C is dependent on the treatment of the infrared region of the integration over the transverse momenta of the emitted gluons, but a physically reasonable choice of the infrared parameter yields an $F_2(x,Q^2)$, in good agreement with the HERA data. The important point is that the value of the exponent $\lambda_L \approx 0.5$ is a stable prediction. That is, the $x^{-1/2}$ *shape* in [16] is a characteristic property of (leading-order) BFKL dynamics; λ_L is not a free parameter, but is determined dynamically. [For this reason we use the subscript L to distinguish the "Lipatov" λ_L from the free parameter λ in Eq. (6).] Of course, the predicted small-x behavior may be modified by subleading corrections. At sufficiently small x, shadowing corrections will almost certainly suppress the growth of F_2 with decreasing x, but this effect is expected to be small in the HERA regime, unless "hot-spot" concentrations of gluons occur within the proton [27]. The non-BFKL term $F_2^{\rm bg}$ is one subleading contribution which may be estimated

$$F_2^{\rm bg}(x,Q^2) \simeq F_2^{\rm bg}(x=0.1,Q^2) \simeq 0.4 \qquad (17)$$

or perhaps rising slowly with decreasing x as implied by the "soft" Pomeron.

We now turn to the second limit, that is, the form of F_2 found at small x and large Q^2/Q_0^2 from the double-leading-logarithm approximation of conventional GLAP evolution. In this case the result depends on the choice of the exponent λ in the input gluon and sea quark distributions

$$xg(x,Q_0^2), xS(x,Q_0^2) \sim x^{-\lambda}\ , \qquad (18)$$

as $x \to 0$. If *nonsingular* input forms are used with $\lambda \leq 0$, then

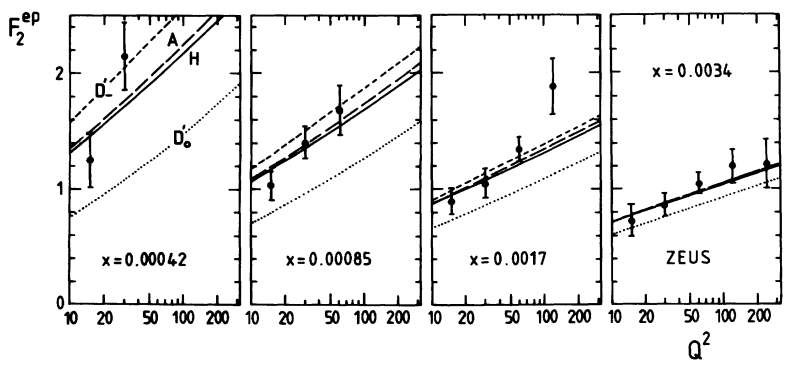

FIG. 10. Description of the preliminary ZEUS measurements [3] of F_2^{ep} for $x < 0.005$ by the parton sets of Refs. [8,10]. The long dashed curves show the fit to the data obtained by the MRS(A) analysis presented in the paper.

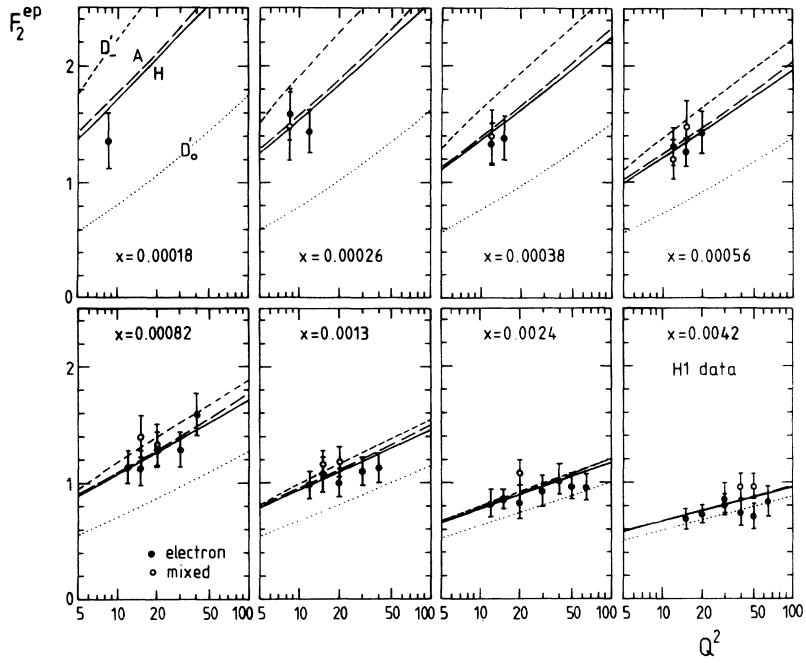

FIG. 11. As for Fig. 10, but showing the preliminary H1 measurements [2].

$$F_2(x,Q^2) \sim \exp(2[\xi(Q_0^2,Q^2)\ln(1/x)]^{1/2}) , \quad (19)$$

where the "evolution length"

$$\xi(Q_0^2,Q^2) \equiv \int_{Q_0^2}^{Q^2} \frac{dq^2}{q^2}\frac{3\alpha_s(q^2)}{\pi} . \quad (20)$$

That is, F_2 increases faster than any power of $\ln(1/x)$, but slower than any power of x. We see that the steepness in x is not stable to evolution in Q^2, but increases rapidly with the evolution length $\xi(Q_0^2,Q^2)$. On the other hand, if *singular* input forms [Eq. (18)] are chosen with $\lambda > 0$, then the $x^{-\lambda}$ shape

$$F_2(x,Q^2) \sim h(Q^2)x^{-\lambda} \quad (21)$$

is stable to evolution in Q^2, and the behavior (21) overrides the double-leading-logarithmic structure of (19) [28].

B. Implications of the global analysis in the HERA regime

Can the HERA measurements of F_2 distinguish between the small-x behaviors presented in (16), (19), and (21), bearing in mind that the data are well described with MRS(A) partons with a sea quark input form

$$xS(x,Q_0^2) \sim x^{-\lambda}(1+\epsilon_S\sqrt{x}+\cdots) , \quad (22)$$

with λ=0.3, and the F_2 mirrors the behavior of xS?

It is informative to first recall the GRV dynamical parton model of Glück, Reya, and Vogt [29], which predated the HERA small-x measurements. GRV predicted a steep behavior of F_2, based on the double-leading-logarithm form (19), by evolving from valencelike input distributions at a very low scale Q_0^2=0.3 GeV^2. Although the GLAP small-x forms of (19) and (21) are quite distinct, in a limited (x,Q^2) region about, say, $(\bar{x},\bar{Q}^2)$ the double-leading-logarithm form mimics as $x^{-\bar{\lambda}}$ behavior with

$$\bar{\lambda} = \left(\frac{36}{b_0}\frac{\ln[\ln(\bar{Q}^2/\Lambda^2)/\ln(Q_0^2/\Lambda^2)]}{\ln(1/\bar{x})}\right)^{1/2} , \quad (23)$$

where, for five flavors, b_0=23 and $\Lambda \approx 150$ MeV. If we were to take Q_0^2=0.3 GeV^2, as in the GRV model [29], then in the HERA regime we have $\bar{\lambda} \gtrsim 0.4$. As we have seen, the HERA data appear to prefer a slightly lower $\bar{\lambda}$. We note that the observed $x^{-0.3}$ behavior can be approximately mimicked if we were to evolve from nonsingular input forms at a higher starting scale of Q_0^2=1 or 2 GeV^2 (see, for example, Ref. [30]).

The detailed x and Q^2 behaviors of the GLAP-based forms (19) and (21) are quite distinct. However, if Q_0^2 is taken as a free parameter in (19) and λ as a free parameter in (21) [or rather in (22)], then the HERA data are not yet precise enough to distinguish between them. It will be even more difficult to distinguish between the BFKL form (16) and the GLAP-based behavior given by (21). In principle, it might appear that the different Q^2 dependences of $C(x,Q^2) \sim (Q^2)^{1/2}$ in (16) and of $h(Q^2) \sim \ln Q^2$ in (21) would be a sufficient discriminator, but in practice the differences are not large [31].

The most distinctive theoretical prediction of this section is the $x^{-\lambda_L}$ behavior with $\lambda_L \simeq 0.5$, embodied in (16), which was obtained from the leading-order BFKL equation. Since λ_L is not a free parameter, the HERA data could have ruled out the precocious onset of this BFKL behavior. Rather, the data are found to be consistent with (16), which may be written in the form

$$F_2 \sim x^{-1/2}(1+ax^{1/2}) , \quad (24)$$

where $a = F_2^{bg}/C$ is weakly dependent on x. At $Q^2 \approx 15$ GeV^2 we estimate[4] that $a \approx 30$. Suppose we approximate the BFKL expectation [Eq. (24)] by the simpler form $F_2 \sim x^{-\lambda}$; then, it follows that

$$\lambda \approx \frac{1}{2} - \frac{ax^{1/2}}{2(1+ax^{1/2})} \approx 0.3 \tag{25}$$

if we insert $a \approx 30$ and a typical value of x in the HERA regime, $x \sim 5 \times 10^{-4}$. That is, the value of λ predicted from BFKL dynamics is in agreement with that found in the global analysis. This very approximate identification at Q^2=15 GeV^2 was simply made to illustrate the similarity of the BFKL description with the global fit based on GLAP evolution. In fact, present data for F_2 cannot distinguish between the two descriptions. An indication of the accuracy required to discriminate between them can be found by comparing the MRS(H) and AKMS curves in Fig. 3 of Ref. [31].

To identify the BFKL behavior (24) with (22), we have used the fact that the ϵ_S term gives a small contribution for $x \sim 10^{-3}$ in the MRS(A) fit. It will be no surprise to report that in the global analysis there is a strong correlation between the values of the λ and ϵ_S parameters in (22). Almost as good a global description of the data can be achieved with, for example,

$$\lambda = 0.2, \quad \epsilon_S = -3.3 \tag{26}$$

or with

$$\lambda = 0.4, \quad \epsilon_S = 2.9\ . \tag{27}$$

In other words, the value of the parameter λ in Eq. (6) is not well determined by the HERA data.

It is important to note that it is the sea quark densities, and not the gluon, which are constrained by the HERA measurements of F_2 at small x. Since the sea quarks are driven by the gluon, via $g \to q\bar{q}$, we have assumed that they have a common $x^{-\lambda}$ behavior at small x [see Eq. (6)]. However, there is, as yet, no experimental confirmation of this assumption, and the ambiguity in the gluon distribution is by far the largest uncertainty in the parton densities. It is therefore crucial to make a direct determination of the gluon in the region $x \lesssim 0.05$. In Sec. V we discuss the gluon distribution in more detail.

To summarize, we find that, within the global analysis, the HERA measurements of F_2 are well fitted by a parametrization which embodies a small-x behavior of the form $F_2 \sim xS \sim x^{-0.3}$. This behavior is consistent with the expectations of BFKL dynamics, as expressed by $F_2 \sim Cx^{-0.5} + F_2^{bg}$ of (16), since this form mimics an $x^{-0.3}$ behavior in the HERA x regime under consideration. The observed $x^{-0.3}$ dependence is, however, not consistent with the GRV "valence" model which gives a steeper behavior in the HERA region (with an effective $\lambda \gtrsim 0.4$). Such an approach could be made consistent with the present data if a higher starting scale Q_0^2 were used to decrease the evolution length. We also noted that very precise measurements of $F_2(x,Q^2)$ at HERA will be needed to distinguish between the BFKL behavior and GLAP evolution from "singular" input distributions (motivated by BFKL dynamics). The converse of this result is of great practical benefit to the determination of partons. It means that we can base the global analysis of the data, including the small-x measurements of F_2, on GLAP evolution (see also Ref. [32]). When precise data for F_2 become available over a range of x and Q^2 in the HERA regime, a global analysis may show a systematic departure from the GLAP forms which would indicate BFKL dynamics and/or the onset of shadowing corrections.

IV. CONSTRAINTS FROM THE ASYMMETRY MEASUREMENTS

As we saw in the Introduction (Figs. 2 and 3), the existing set of partons, MRS(H), and its counterpart CTEQ2M do not simultaneously describe the Drell-Yan and W rapidity asymmetry measurements. This is one of the major motivations to redo the global analysis incorporating these data and to present a new set of partons, MRS(A), which rectifies the deficiency. The improvement is shown by the MRS(A) curves in Figs. 2 and 3.

A. Drell-Yan asymmetry

We have seen, from inspection of (11)–(14) that the "core" deep-inelastic structure function data offer little constraint on $\bar{d} - \bar{u}$. An indication that $\bar{d} \neq \bar{u}$ came from the NMC evaluation [13] of the Gottfried sum

$$I_{GS} \equiv \int_0^1 \frac{dx}{x}(F_2^{\mu p} - F_2^{\mu n}) = \tfrac{1}{3} - I_{sea}\ , \tag{28}$$

where the last equality separates the sum into a valence and a sea quark contribution. NMC directly measured the integral over the interval $0.004 < x < 0.8$ and found 0.236 ± 0.008 (stat) [13]. If we correct for deuteron screening effects and assume reasonable extrapolations over the unmeasured x intervals, then the NMC result implies

$$I_{sea} \equiv \frac{2}{3}\int_0^1 (\bar{d} - \bar{u})dx \approx 0.1 \tag{29}$$

for $Q^2 \sim$ 4–7 GeV^2. This constraint on $\bar{d} - \bar{u}$ given by (29), which is sensitive to the assumption made for the small-x behavior of the valence quarks, is not (and should not be) directly included in the global analysis. Our fit already includes the NMC data on which the model-dependent result (29) is based.

The asymmetry in Drell-Yan production in pp and pn

[4]The most recent Askew-Kwieciński-Martin-Sutton (AKMS) [27] description (16) of HERA data (which can be found in Ref. [31]) has the approximate form $F_2 = 0.018x^{-1/2} + 0.385(x/x_0)^{-0.08}$ at Q^2=15 GeV^2, where x_0=0.1. Thus we have $a \equiv F_2^{bg}/C \approx 0.6/0.018 \approx 30$ for x in the HERA regime ($x \sim 5 \times 10^{-4}$).

collisions offers a direct determination of $\bar{d}-\bar{u}$ [12]. The sensitivity can be seen from the leading-order expression

$$A_{\rm DY} \equiv \frac{\sigma_{pp}-\sigma_{pn}}{\sigma_{pp}+\sigma_{pn}} = \frac{(u-d)(\bar{u}-\bar{d})+\frac{3}{5}(u\bar{u}-d\bar{d})}{(u+d)(\bar{u}+\bar{d})+\frac{3}{5}(u\bar{u}-d\bar{d})+\frac{4}{5}(s\bar{s}+4c\bar{c})}\ , \quad (30)$$

where $\sigma \equiv d^2\sigma/dM\,dy|_{y=0}$ and where the partons are to be evaluated $x=\sqrt{\tau}=M/\sqrt{s}$; M and y are the invariant mass and rapidity of the produced lepton pair. Since $u>d$ in the proton, the asymmetry is positive for parton sets with $\bar{d}-\bar{u}$ zero or small, but becomes negative as $\bar{d}-\bar{u}$ increases.

When we include the recent NA51 asymmetry measurement [4] $A_{\rm DY}=-0.09\pm0.02\pm0.025$ at x=0.18 in the next-to-leading-order analysis, the description of the data is shown by the MRS(A) curve in Fig. 2. Figure 12 shows that the introduction of the NA51 measurement leads to a significant increase in $\bar{d}-\bar{u}$ in going from the "old" MRS(H) to the "new" MRS(A) partons. In the region $0.02\lesssim x\lesssim 0.7$, where a full set of deep-inelastic data exists, we expect the MRS(A) partons to be very similar to those of MRS(H), except that $\bar{d}-\bar{u}$ would be much larger while at the same time approximately conserving $\bar{u}+\bar{d}$, $d+\bar{d}$, and $u+\bar{u}$ [as expected from (11)–(14)]. Thus we anticipate an increase of $\bar{d}$ which is compensated by a corresponding decrease in $\bar{u}$ and d, which in turn requires a similar increase in u. The picture is a bit too simplistic since there are new NMC data in the MRS(A) fit, and moreover we have to maintain the description of the W rapidity asymmetry measurements. Nevertheless, the comparison of the MRS(A) and MRS(H) shown in Fig. 13 displays the trends that we expect.

The NA51 collaboration also measured the asymmetry A_ψ of J/ψ production in pp and pn collisions. Now J/ψ production can be of gg, as well as $q\bar{q}$, origin. We may use a simple model [33], in which

$$\hat{\sigma}(gg\to\psi)=r\hat{\sigma}(q\bar{q}\to\psi)\ , \quad (31)$$

where r=0.5, to estimate the asymmetry. This value of r is obtained by comparing the rate of J/ψ production in

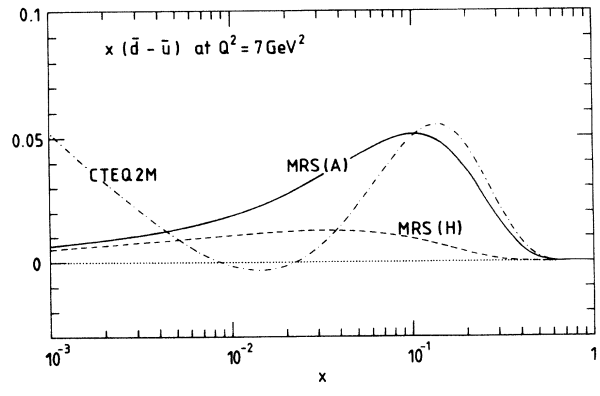

FIG. 12. $x(\bar{d}-\bar{u})$, as a function of x, at Q^2=7 GeV^2 obtained from the MRS(H) [10], CTEQ2M [11], and the new MRS(A) sets of partons.

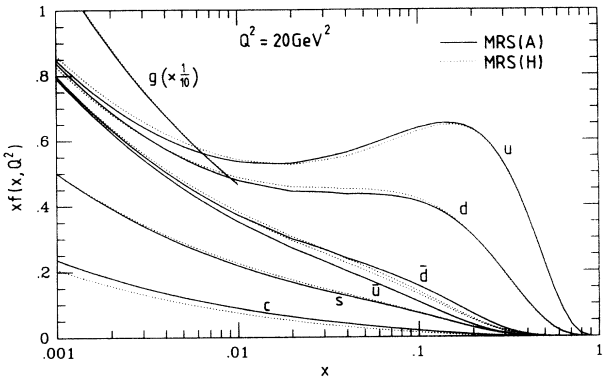

FIG. 13. Comparison of Q^2=20 GeV^2 of the new MRS(A) partons of this analysis and the MRS(H) partons of Ref. [10].

pp and $p\bar{p}$ collisions [33]. To leading order we have

$$A_\psi = \frac{\sigma_{pp}(\psi)-\sigma_{pn}(\psi)}{\sigma_{pp}(\psi)+\sigma_{pn}(\psi)} = \frac{(u-d)(\bar{u}-\bar{d})}{rgg+(u+d)(\bar{u}+\bar{d})+2s\bar{s}+2c\bar{c}}\ , \quad (32)$$

where $\sigma \equiv d\sigma/dy|_{y=0}$ and where the partons densities are evaluated at $x=M_\psi/\sqrt{s}$ and $Q^2=M_\psi^2$. In principle, it appears that a measurement of A_ψ offers a more direct determination of $(\bar{u}-\bar{d})$ than $A_{\rm DY}$, but in practice the gg term dominates and considerably dilutes the predicted asymmetry A_ψ. As a consequence, the NA51 measurement [4] $A_\psi=-0.03\pm0.002$ (stat)$\pm$0.02 (syst) is not able to distinguish between the different sets of partons. However, the value $A_\psi=-0.013$ predicted using the MRS(A) partons is consistent with the measured value.

B. W charge asymmetry

The $W^\pm$ charge asymmetry at the Fermilab $p\bar{p}$ collider,

$$A_W(y)=\frac{d\sigma(W^+)/dy-d\sigma(W^-)/dy}{d\sigma(W^+)/dy+d\sigma(W^-)/dy}\ , \quad (33)$$

is a sensitive probe of the difference between u and d quarks in the $x\sim0.1$, $Q\sim M_W$ region. Because the u quarks carry more momentum on average than the d quarks, the W^+ tend to follow the direction of the incoming proton and the W^- that of the antiproton, i.e., $A_W>0$ for $y>0$. Thus a precise measurement of the W asymmetry—in practice the asymmetry A_l of the charged lepton from W decay (5)—serves as a valuable independent check on the u- and d-quark distributions. There is a direct correlation between the lepton asymmetry and the *slope* of the d/u ratio. To see this we first note that the dominant contribution to W^+ (W^-) production comes

from the $u\bar{d}$ ($d\bar{u}$) annihilation process. Thus

$$A_W(y) \simeq \frac{u(x_1)d(x_2) - d(x_1)u(x_2)}{u(x_1)d(x_2) + d(x_1)u(x_2)} , \qquad (34)$$

where the scale $Q = M_W$ is implicit for the parton distributions, and

$$x_{1,2} = x_0 \exp(\pm y), \quad x_0 = \frac{M_W}{\sqrt{s}} . \qquad (35)$$

If we introduce the ratio $R_{du}(x) = d(x)/u(x)$, then, for small y,

$$A_W(y) \simeq -x_0 y \frac{R'_{du}(x_0)}{R_{du}(x_0)} . \qquad (36)$$

In reality, the situation is of course more complicated—it is the *lepton* asymmetry (5) which is measured, and there are subleading and higher-order corrections to Eq. (34). Nevertheless, the correlation implied by Eq. (36) *is* evident in the full prediction.[5] Figure 14 shows the MRS(A), MRS(H), and CTEQ2M u, d, and d/u parton distributions as a function of x at $Q^2 = M_W^2$. The x range is chosen to correspond to the lepton asymmetry measurement by CDF at the Fermilab $p\bar{p}$ collider [5]. The slope of d/u is significantly larger in magnitude for the CTEQ set, and this leads to the larger lepton asymmetry shown in Fig. 3. MRS(H) partons give an excellent description of the W asymmetry, in fact slightly better (in terms of χ^2) than MRS(A), which includes the data in the fit. For this reason u and d do not change as much as might be expected to compensate for the increase in $\bar{d} - \bar{u}$ in going from MRS(H) to MRS(A) [see Fig. 13 and the discussion following Eqs. (11)–(14)].

From Fig. 3 we can conclude that CTEQ2M is ruled out by the data. This illustrates the discriminating power of the CDF data, since CTEQ2M is consistent with all the deep-inelastic scattering data and with the NA51 Drell-Yan asymmetry. It is interesting to note that the CTEQ2M gives a reasonable description of the NMC F_2^n/F_2^p data [21] shown in Fig. 7, a quantity which is also correlated with the d/u ratio. The reason that there is no contradiction between this and the misfit of the CDF asymmetry data is that the n/p ratio is more influenced by the $\bar{u}$ and $\bar{d}$ distributions than is σ_W—the former is, in a sense, *linear* in the small-$\bar{q}/q$ correction, $F_2^p \sim \frac{4}{9}(u+d) + \frac{4}{9}(\bar{u}+\bar{d})$, whereas the latter is *quadratic*, $\sigma(W^+) \sim u\bar{d} + d\bar{u}$. Hence the W asymmetry is a more direct probe of the d/u ratio than the n/p structure function ratio. The "incorrect" d/u ratio of CTEQ2M is compensated by the antiquark contributions in the fit to the n/p ratio. Early work on the interconnection between the W asymmetry, the d/u ratio, and the n/p structure function ratio can be found in Refs. [35,36].

[5]The curves in Fig. 3 are calculated using the next-to-leading-order program DYRAD of Ref. [34]. We thank Nigel Glover for helping with these calculations of the W asymmetry.

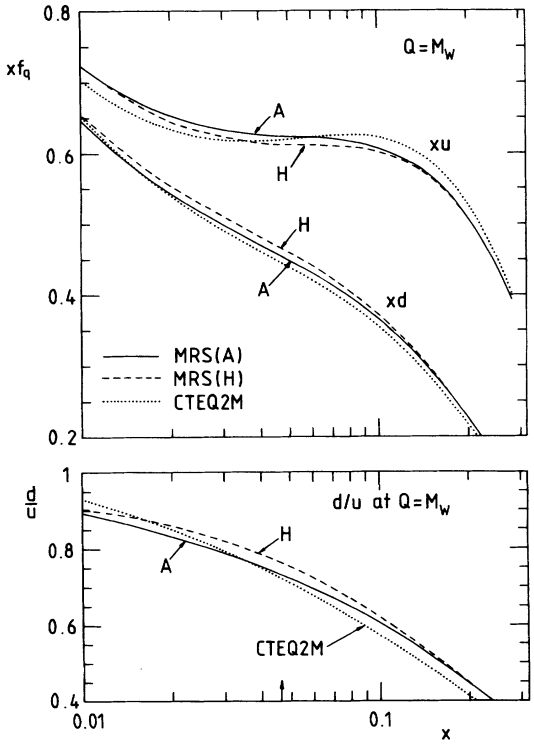

FIG. 14. u, d, and d/u distributions at $Q^2 = M_W^2$ obtained from the MRS(H) [10], CTEQ2M [11], and the new MRS(A) sets of partons.

Another place where the d/u ratio is important is in the precision W mass determination in $p\bar{p}$ collisions. Because of the finite rapidity acceptance of the experiments, the lepton transverse momentum spectrum, from which the mass is determined, depends on the shape of the rapidity distribution of the W [36]. Once again, the correlation is with the d/u ratio and, hence, the W asymmetry can be used to rule out sets of parton distributions in the M_W analysis. In fact, it should be possible to produce sets of distributions which give "$\pm 1\sigma$" fits to the W asymmetry data of Fig. 3 and to use these to infer a $\pm 1\sigma$ error on M_W from parton distributions.[6] We shall return to this issue in a future study.

V. GLUON DISTRIBUTION

The new data which we have introduced into the global analysis has enabled us to fine-tune the *quark* distributions. In this section we comment briefly on the status of and prospects for information on the *gluon* distribution.

The only precise information on the gluon distribution is that the total momentum fraction is about 43% at $Q^2 = Q_0^2$ (Table III). Traditionally, information on the gluon *shape* has come directly from large-p_T prompt photon production in fixed-target pN collisions, where

[6]We are grateful to Arie Bodek and David Saltzberg for discussions on this point.

the $qg \to \gamma q$ process is dominant. In particular, past and present MRS distributions have used the high-precision WA70 $pp \to \gamma X$ data [24] to constrain the shape of the gluon in the $x \sim 0.3$–0.4 region. Other experiments have of course measured prompt photon production, but for the most part these are unable to provide any useful additional constraints, either because of the size of the error bars or because they involve heavy targets. Only the recent pp data from the UA6 experiment [37] are competitive with those of WA70, and these will be incorporated in a future study of the uncertainty in the gluon distribution. In the meantime we have checked that the MRS(A) gluon distribution is consistent with that extracted by UA6 themselves. Although there are now prompt photon data from the CERN and Fermilab $p\bar{p}$ colliders, only the small-p_T part of the distributions, where the $qg \to \gamma q$ subprocess dominates, is sensitive to the gluon distribution. It is in this region, however, that the experimental and theoretical uncertainties are largest (see below). Indirect information also comes from scaling violations in fixed-target deep-inelastic scattering, where the gluon gives an important contribution to the Q^2 dependence particularly at small x.

In previous studies [38], we have investigated the interplay between the prompt photon and deep-inelastic data and derived "$\pm 1\sigma$" gluons which attempted to span the allowed range of the distribution at medium to large x. We should stress that all our recent distributions, for example, MRS(D_0',D_-',H,A), are global "best fits" to the data (available at the time of the analysis) of all the processes listed in Table I. The HERA measurements of F_2 were not available for the MRS(D) analyses, but these data do not pin down the gluon, and so D_0' and D_-' can be used to demonstrate the ambiguity in its behavior. However, the point we wish to emphasize is that the recent global analyses are "best fits" to the WA70 data, and so the spread of the gluons obtained underestimates the uncertainty. Nevertheless, it is interesting to compare the variation in the recent MRS gluon distributions. Figure 15 shows the D_0', D_-', and A gluons[7] at Q^2=20 GeV^2. We see immediately that there are regions in x where these are very different (note the logarithmic scale) and regions where they are quite similar. We discuss these in turn below.

(i) At *very small* x, $x \lesssim 0.01$, the size and shape of the gluon is controlled by the $x^{-\lambda}$ term in the starting parametrization. Since the gluons are constrained to be similar at larger x (see below), a larger λ implies a steeper, larger gluon in the very-small-x region. As discussed in detail in Sec. III, perturbative QCD (whether manifest in GLAP or BFKL dynamics) always ties the small-x behavior of the sea quarks and gluons together, and in the MRS fits we always use the same λ parameter for both [see Eq. (6)]. Thus the spread of the D_0', D_-', and A gluons in Fig. 15 is very similar to that in the corresponding F_2's at small x. Note, however, that while we would expect the ratio $\bar{q}/g$ to be approximately constant as $x \to 0$, we cannot say at which value of x this constancy should set in. In fact, for MRS(A) this proportionality between the distributions is valid over a broad range of small x, since the ϵ_S term turns out to be comparatively small in the sea-quark distribution and since there is no such parameter in the gluon distribution,[8] i.e., $\epsilon_g \equiv 0$ [Eq. (6)].

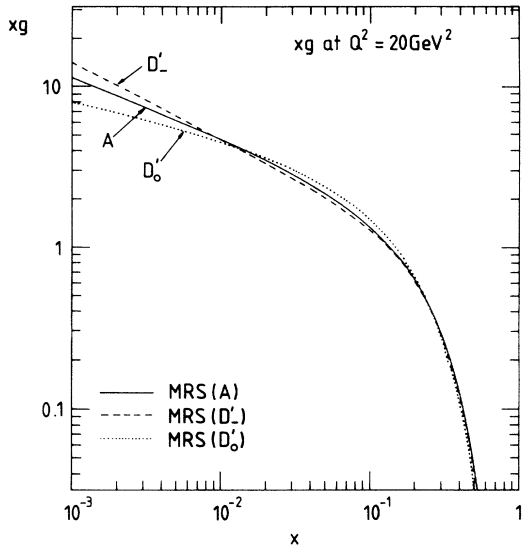

FIG. 15. Gluon distributions from sets D_0' (dotted curve), D_-' (dashed curve), and A (solid curve) at Q^2=20 GeV^2.

Now that the very-small-x quarks are being pinned down by the HERA data, it is important to measure the gluon at small x to look for evidence of a steeply rising distribution. Various methods have been suggested for directly extracting the gluon distribution at HERA. Possible structure function determinations are the measurement of the longitudinal structure function F_L [39] and of the derivative $dF_2/d\ln Q^2$, both of which are dominated by a term proportional to the gluon at small x. Figure 16 shows xg, F_L, and $dF_2/d\ln Q^2$ at small x for the D_0', D_-', and A partons. Also shown are the first data on the F_2 slope from H1 [40]. The size of the error bars prevents any conclusions from being drawn at present.

The production of large-p_T jet pairs with large rapidity at the Fermilab $p\bar{p}$ collider has also been suggested as a way of probing the very-small-x distribution [41,42]. Preliminary indications appear to favor a steeply rising gluon, although a more complete study of the experimental systematic errors and of the next-to-leading-order QCD corrections is required before any definite conclusions can be drawn.

(ii) At *medium-large* x, $\sim 0.2 < x \lesssim 0.4$, the gluon distributions in Fig. 15 are constrained by the prompt photon data and are therefore similar. This is *not* to say that there is no uncertainty in the gluon this region—in fact,

[7]The A and H gluons are essentially identical (see Fig. 13).

[8]Our approach has always been to use simple, physically motivated forms for the starting distributions and to only introduce extra parameters as and when required by the data.

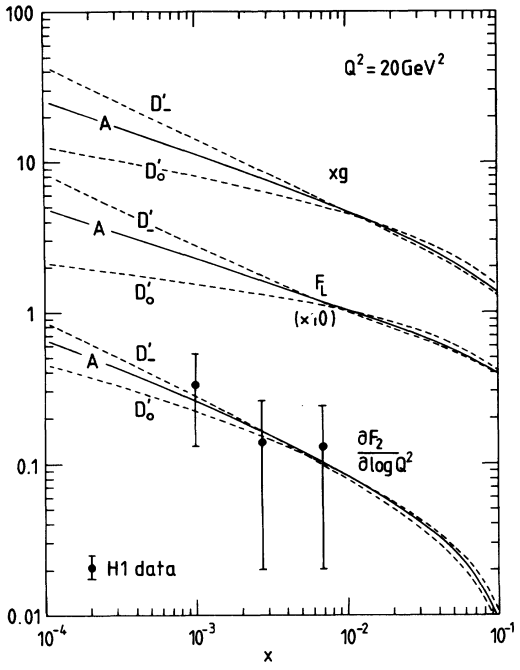

FIG. 16. Gluon distributions and the corresponding predictions for $dF_2/d\ln Q^2$ and F_L for the D'_0,D'_- (dashed lines) and A (solid line) parton distributions, together with data from H1 [40].

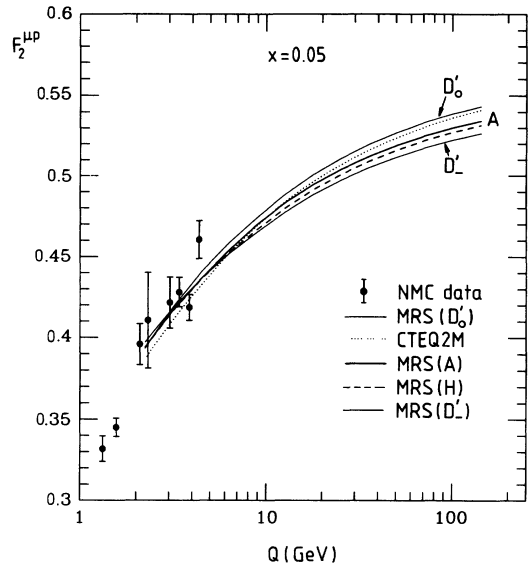

FIG. 17. Structure function F_2^p at x=0.05 as a function of Q, with data from NMC [6] and the descriptions of the MRS(D'_0,D'_-, A,H) and CTEQ2M partons.

quite a large spread is allowed by the error bars on the data and by the factorization and scale dependence of the next-to-leading-order QCD cross section [38]. Roughly speaking, this translates into an order ± 1 uncertainty on the power η_g of $(1-x)$. Note that in the MRS parametrization of the gluon [Eq. (6)] the parameter γ_g compensates the different small-x behaviors in, for example, D'_0, D'_-, and A, leading to roughly equal distributions with the same parameter η_g at larger x. The larger the value of λ, the bigger is the corresponding value of γ_g.

(iii) At *very large* x, $x \gtrsim 0.4$, there are essentially no constraints on the gluon distribution. Phenomenologically, this region is of little importance for high-energy hadron-hadron colliders. It is interesting, however, that the power of $(1-x)$ determined by the prompt photon data at medium-large x, η_g=5.3 for MRS(A) at Q_0^2=4 GeV^2, is perfectly consistent with the naive expectation from dimensional counting, η_g=5, which is supposed to be valid in the limit $x \to 1$ at some low-Q^2 scale.

(iv) The *medium-small-x* region $\sim 0.01 < x \lesssim 0.2$ is perhaps the most interesting of all. Because of (a) the momentum sum rule and (b) the requirement of similar gluons at larger x, and gluon distribution which is much larger at very small x must be smaller in this region. This leads to a crossover point at around $x \sim 0.01$ for the gluons shown in Fig. 15. One direct consequence of this is that, in this region of x, structure functions such as F_2 evolve more slowly with Q^2 for sets with "singular" gluons at very small x. This is illustrated in Fig. 17, which shows F_2^p at x=0.05 as a function of Q, with data from NMC [6] and curves corresponding to the MRS(D'_0,D'_0,A,H) and CTEQ2M partons. The fits are, of course, constrained to be in agreement in the Q range where accurate NMC data are available. Note, however, the divergence of the predictions as Q increases. This is directly related to the magnitude of the gluons in this region of x and Q, as is evident from Fig. 18, which shows the corresponding gluons at the same value of x as a function of Q. The effect of the gluon on the evolution

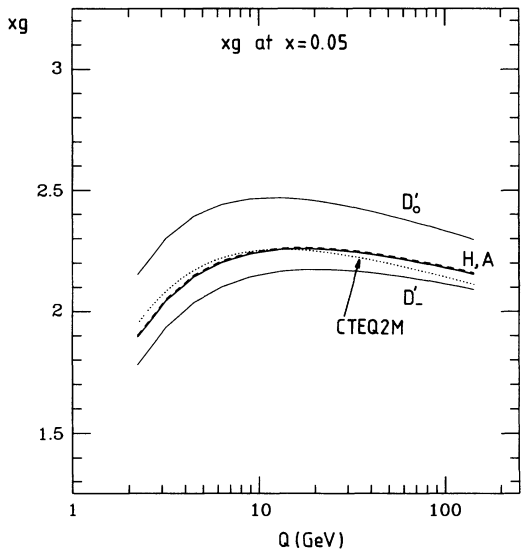

FIG. 18. Gluon distributions $xg(x,Q^2)$ of the MRS(D'_0,D'_-,A,H) and CTEQ2M partons, at x = 0.05, as a function of Q.

of the quark distributions at medium-small x has important consequences for W and Z physics at the Fermilab $p\bar{p}$ collider. This will be discussed in more detail in the following section.

There are, in fact, several hard scattering processes at the Fermilab collider which offer, at least in principle, the possibility of measuring the gluon distribution in the medium-small-x range. Data on prompt photon production in the range 10 GeV/$c \lesssim p_T^\gamma \lesssim$100 GeV/$c$ have recently become available [43]. Next-to-leading-order predictions using "standard" gluon sets give a reasonable description of the data for $p_T^\gamma \gtrsim$30 GeV/c [43]. Below this value the measured cross section rises slightly more rapidly than the predictions, indicating an excess of data over theory. However, this is precisely the region where (a) the uncertainties due to scale dependence and to matching the theoretical and experimental definitions of "isolated" photons are greatest and (b) one expects significant contributions from higher-order processes, in particular those involving the photon fragmentation function. Although steeply rising distributions such as those of MRS(D'_) and GRV [29] appear to do slightly better in describing the small-p_T^γ data [44], it seems premature to include these data in the global fit. For example, artificially enhancing the gluon to fit the CDF low-p_T^γ data, at the same time keeping the overall gluon momentum fraction fixed, inevitably depletes the large-x part of the distribution, thus spoiling the fit to the WA70 data.[9]

The $b\bar{b}$ cross section, being proportional to the square of the gluon distribution, is also of potential importance. Again, unfortunately, there are substantial theoretical uncertainties arising from a large-scale dependence and experimental uncertainties in reconstructing the total cross section from the measured distributions of B mesons, leptons, J/ψ's, etc., in restricted kinematic ranges (see, for example, Ref. [45]). Also, $b\bar{b}$ production at the Fermilab $p\bar{p}$ collier samples x values ($x \lesssim 0.01$) just below the crossover point where the various gluons have similar magnitudes (see Fig. 15). The most recent indications [46] are that while there is no serious disagreement between theory and experiment, the uncertainties are still much too large to allow any discrimination between gluon distributions at the level required by Fig. 15.

In summary, there is still a considerable amount of uncertainty in the gluon distribution, particularly in the important medium-small- and very-small-x regions. HERA will eventually provide information on the latter, and in the meantime large rapidity jet and prompt photon production at the Fermilab $p\bar{p}$ collider are beginning to provide useful constraints. Current studies tend to use sets such as MRS(D_0') and MRS(D'_) to quantify the effect of different small-x gluon shapes on cross section predictions, even though the corresponding quark distributions are now ruled out by the HERA F_2 data. In a future study, we will explore the possibilities for varying the gluon distribution while maintaining a good fit to the structure function data.

[9]We are grateful to Steve Kuhlmann for discussions on this point.

VI. HADROPRODUCTION OF W BOSONS AND TOP QUARKS

In this section we present predictions for the total W and $t\bar{t}$ cross sections in $p\bar{p}$ collisions at 1.8 TeV. The former is being measured more and more precisely by both CDF and D0 and already provides a valuable cross-check on the size of the u and d distributions. Interest in the latter has recently been rekindled by the evidence for top production presented by the CDF collaboration [51], with the suggestion that the measured production cross section is larger than the theoretical prediction.

A. W production cross section

While the W asymmetry probes the relative size of the u and d distributions, the *total* cross sections for W and Z boson production in $p\bar{p}$ collisions at $\sqrt{s}$=1.8 TeV provide an important check of the overall magnitude of the quark distributions in a region of x where they are constrained by deep-inelastic (mainly NMC and CCFR) data. Since the subprocess cross section is known to next-to-next-to-leading order [47], there is very little theoretical uncertainty in the predictions once the parton distributions are specified.

To illustrate this, we show in Fig. 19(a) the total W production cross section for the MRS(A,H,D_0',D'_) and CTEQ2M parton distributions. The central points are calculated assuming M_W=80.21 GeV/c^2 and setting the

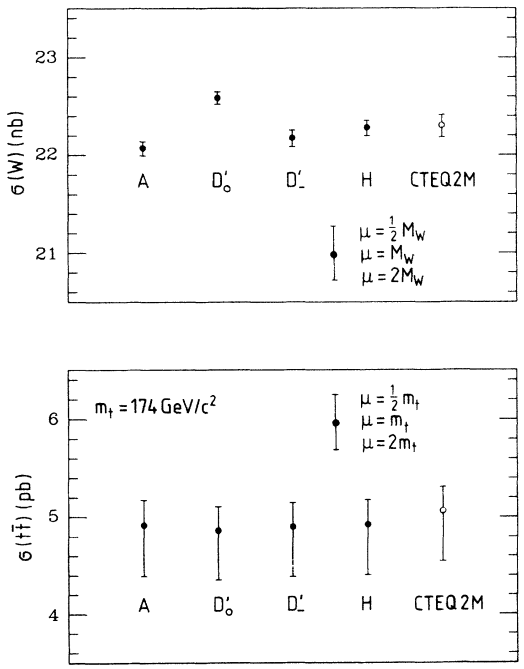

FIG. 19. (a) Predictions for σ_W and (b) $\sigma_{t\bar{t}}$ (m_t=174 GeV/c^2) in $p\bar{p}$ collisions at $\sqrt{s}$=1.8 TeV, from the MRS(D_0',D'_,A,H) and CTEQ2M partons. The central values are calculated using renormalization and factorizations scales equal to (a) M_W and (b) m_t, and the error bars indicate the effect of increasing and decreasing these by a factor of 2.

renormalization and factorization scales equal to M_W. The error bars show the effect of changing both scales simultaneously by a factor of 2. The first point to note is that the σ_W predictions for MRS(A), MRS(H), and CTEQ2M are very similar. (Note also the scale dependence is weak and gives a similar variation in cross section as the spread in the three predictions.) This can be understood by recalling that σ_W is largely determined by the product $u(x_W, M_W^2)d(x_W, M_W^2)$, where $x_W = M_W/\sqrt{s} \sim 0.05$. By comparing the relative size of the u and d distributions for the MRS(A), MRS(H), and CTEQ2M sets (Fig. 14), we can understand the similarity of the corresponding σ_W predictions shown in Fig. 19(a). First, we have that

$$\left.\begin{array}{l} u(\mathrm{A}) > u(\mathrm{H}) \\ d(\mathrm{A}) < d(\mathrm{H}) \end{array}\right\} \Rightarrow \sigma_W(\mathrm{A}) \simeq \sigma_W(\mathrm{H}) \ . \qquad (37)$$

The situation with CTEQ2M is more subtle. By comparing the u and d distributions at x_W, we could conclude that

$$\left.\begin{array}{l} u(\mathrm{A}) \simeq u(\mathrm{2M}) \\ d(\mathrm{A}) > d(\mathrm{2M}) \end{array}\right\} \Rightarrow \sigma_W(\mathrm{A}) > \sigma_W(\mathrm{2M}) \ , \qquad (38)$$

whereas in fact the reverse is true. The reason lies in the different shapes of the W rapidity distributions. The CTEQ2M W cross section receives a significant contribution from W^+ (W^-) produced at large positive (negative) rapidity, where a large-x u quark interacts with a small-x d quark. Especially for the former, the CTEQ2M distribution is significantly larger than the MRS(A) distribution (see Fig. 14), giving a distinctly different W rapidity distribution, as shown in Fig. 20 for $p\bar{p} \to W^+ + X$. This is, of course, the origin of the much too large CTEQ2M lepton rapidity asymmetry discussed in Sec. IV B and shown in Fig. 3. Comparing MRS(A) and MRS(H), we see that the distribution in y_W for the latter is slightly larger for $y_W < 0$, which is reflected in the total cross section shown in Fig. 19(a). Since the $\Lambda_{\overline{\mathrm{MS}}}$ values and gluon distributions (for $x \sim x_W$; see Fig. 18) for these three sets are very similar, the above orderings of u and d at $Q = M_W$ simply reflect the orderings at the lower scales where the distributions are constrained by the fixed-target deep-inelastic and asymmetry data discussed in the previous sections. Of the three sets, only MRS(A) gives a consistent fits to *all* the data, and so we may conclude that σ_W(A) is the most accurate prediction.

It is also worth commenting on the differences between the MRS(H), MRS(D$_0'$), and MRS(D$_-'$) W cross sections.

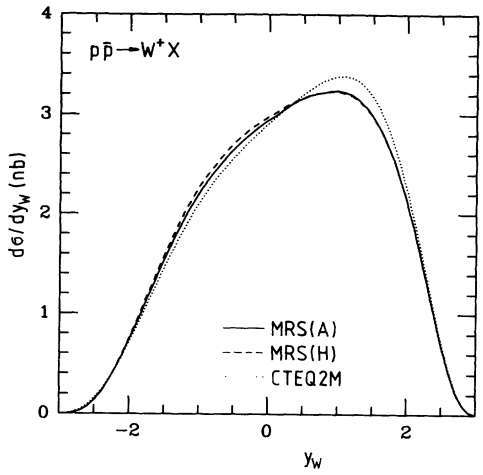

FIG. 20. Next-to-leading-order predictions for W^+ rapidity distribution in $p\bar{p}$ collisions at $\sqrt{s}$=1.8 TeV from the MRS(A,H) and CTEQ2M partons.

The three parton sets have similar u- and d-quark distributions for $x \sim x_W$ and Q^2 values characteristic of the fixed-target deep-inelastic scattering data [10]. There is, however, a rather large spread in the corresponding W cross sections shown in Fig. 19(a). These differences arise from the different *gluon* distributions in the three sets. We have seen in the previous section that $x \sim 0.05$ is precisely the region where the gluon is not well constrained. Thus, even though the quarks are accurately determined at low Q for this x range, differences in the gluon can affect the GLAP evolution to $Q = M_W$ and lead to differences in the quarks at this scale. This is graphically illustrated by the σ_W(H), σ_W(D$_0'$), and σ_W(D$_-'$) predictions shown in Fig. 19(a). From Fig. 18 we see that the ordering of the gluons at low Q and x=0.05 is g(D$_-'$) < g(H)< g(D$_0'$), and hence the quarks of D$_-'$ or D$_0'$ increase more slowly or rapidly than those of H. This leads directly to σ_W(D$_-'$) < σ_W(H)< σ_W(D$_0'$). It would appear, therefore, that now that the quarks are very well constrained, it is the uncertainty in the gluon distribution around $x \sim 0.05$ which constitutes the largest theoretical uncertainty in the predictions for the W (and Z) cross sections at the Fermilab $p\bar{p}$ collider.

A precision measurement of σ_W at the percent level would obviously provide a useful additional constraint on the distributions. The most recent values [48,49] for σ_W are[10]

$$\begin{aligned} \mathrm{CDF}(e,\mu): \ \ & \sigma_W = 20.4 \pm 0.4 \ (\mathrm{stat}) \pm 1.2 \ (\mathrm{syst}) \pm 1.4 \ (\mathrm{lum}) \ \mathrm{nb} \ ; \\ \mathrm{D0}(e,\mu): \ \ & \sigma_W = 19.0 \pm 0.6 \ (\mathrm{stat+syst}) \pm 2.3 \ (\mathrm{lum}) \ \mathrm{nb} \ . \end{aligned} \qquad (39)$$

We should note that these cross sections relied on a luminosity measurement which has since been superseded by a new measurement of the total $p\bar{p}$ cross section by CDF [50]. If the new values are indeed some 10% higher, as

[10]We have divided out the standard model leptonic branching ratio $B(W \to l\nu)$=0.108.

suggested by the ratio of "new" and "old" total cross section measurements, then this would bring them more into line with the theoretical predictions shown in Fig. 19(a). However, the errors on the data in Eq. (39) are still much too big to provide the level of discrimination between the distributions discussed above. Indeed, the accuracy of the theoretical prediction suggests that the W cross section could itself serve as a determination of the collider luminosity.

Finally, we note that HERA will eventually be able to make a reasonably precise measurement of F_2^p in a region of Q intermediate between the fixed target data and M_W (see Fig. 17). In fact, the first data in this kinematic region have recently been presented by H1 [2] and ZEUS [3], although the error bars are so large that no meaningful discrimination between the predictions is possible at present.

B. $t\bar{t}$ production cross section

The evidence presented recently by the CDF Collaboration [51] has focused attention on the theoretical prediction for the top quark production cross section. Here we address the question of the uncertainty in the calculation of $\sigma_{t\bar{t}}$ coming from parton distributions. Figure 19(b) shows the next-to-leading-order QCD predictions [52] for the total cross section for m_t=174 GeV/c^2, the central value reported by CDF, with the factorization and renormalization scales set equal to m_t. The error bars on the predictions indicate the effect of changing the scales by a factor of 2. The relative spread in the predictions is somewhat less than for σ_W, since now the quark distributions are being probed in the range of $x \sim 0.2$–0.4, where the high-statistics BCDMS and CCFR data provide a very tight constraint.[11] The more important point, however, is that unlike for σ_W, the dominant effect is the scale dependence. As discussed in detail in Ref. [52], this scale dependence is symptomatic of large contributions to the cross section from soft gluons at higher orders in perturbation theory. Figure 21 shows the next-to-leading-order prediction for $\sigma_{t\bar{t}}$ as a function of m_t using the MRS(A) partons. The solid curve corresponds to the scale choice $Q = m_t$ and the dashed curves to $Q = 2m_t, \frac{1}{2}m_t$. The data point is the CDF measurement [51] $\sigma_{t\bar{t}} = 13.9^{+6.1}_{-4.8}$ pb for $m_t = 174 \pm 17$ GeV/c^2.

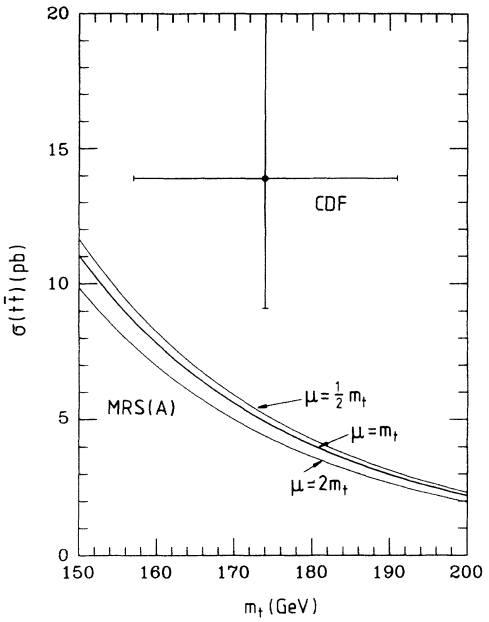

FIG. 21. Next-to-leading-order predictions for $\sigma_{t\bar{t}}$ at $\sqrt{s}$=1.8 TeV as a function of m_t using MRS(A) partons. The curve is calculated using renormalization factorization scales equal to m_t, and the band corresponds to changing scales to $\frac{1}{2}m_t$ and $2m_t$. The data point is from the CDF Collaboration [51].

VII. CONCLUSIONS

To determine the partonic structure of the proton, we have performed a global next-to-leading-order analysis of the data for deep-inelastic scattering and related hard scattering processes. We summarized the constraints on the partons arising from the various types of data in Table I. We found that a surprisingly economical parametrization of the parton densities at Q^2=4 GeV^2 was able to give a satisfactory description of this wide range of data. We were able to include in the analysis for the first time significant new measurements of F_2 at HERA, of the asymmetry $A_{\rm DY}$ in Drell-Yan lepton-pair production from pp and pn collisions and of the $W^{\pm}$ rapidity asymmetry A_W at Fermilab. The partons that we obtain, MRS(A), are the only set which is consistent with all the data.[12] (The only exception which remains is the incompatibility with the lowest-x measurements by CCFR of the neutrino structure functions F_2 and xF_3.)

The asymmetry data considerably tighten the constraints on the u, d, $\bar{u}$, and $\bar{d}$ distributions. In particular, the NA51 measurement of $A_{\rm DY}$ provides "missing" information—it pins down the combination $\bar{d}-\bar{u}$, which is essentially undetermined by the deep-inelastic structure function measurements. On the other hand, the measurements of the $W^{\pm}$ lepton rapidity asymmetry provide a tight constraint on the ratio d/u, with $\bar{u}$ and $\bar{d}$ having less influence in this case.

An interesting feature to emerge from the analysis is the nature of the link between the u and d distributions at $Q^2 \sim M_W^2$ and $x \sim 0.05$, which determine the W cross section at Fermilab, and the u and d densities determined from the fixed-target data with $Q^2 \sim 20$ GeV^2. Even for x

[11] Note that the $q\bar{q}$ annihilation process accounts for approximately 90% of the total cross section for this value of m_t.

[12] The FORTRAN code for the MRS(A) set is available by electronic mail from W.J.Stirling@durham.ac.uk

as large as 0.05, the evolution from $Q^2 \sim 20$ GeV^2 to M_W^2 is found to depend appreciably on the gluon distribution, particularly in the initial stages of the evolution.

The measurements of F_2 at HERA have opened up the small-x regime, $x \lesssim 10^{-3}$. The dramatic growth of F_2 observed with decreasing x, which has been anticipated in perturbative QCD models, is readily accommodated in the global fit. Indeed, we found that the observed small-x behavior is entirely consistent with the precocious onset of BFKL leading-$\ln(1/x)$ dynamics, although alternative QCD explanations are not ruled out.

We believe that our analysis has considerably improved the detailed knowledge of the quark densities. However, the same is not true for the gluon distribution. At present there are, with the possible exception of the WA70 prompt photon measurements, no reliable direct constraints on the gluon. In principle, $b\bar{b}$ and jet production cross sections depend directly on the gluon density, but ambiguities, as a result of scale dependence, jet recognition, higher-order effects, the choice of m_b, etc., mean that so far these data have provided little additional information on the gluon. Valuable indirect constraints on the gluon come from the momentum sum rule and from the observed structure of the deep-inelastic scaling violations. Our philosophy has been to keep the parametrization of the partons as economical as possible and to only introduce an extra parameter when it is required to improve the description of the data. For this reason the parametrization of the gluon is remarkably simple, such that its behavior is prescribed by the momentum sum rule and the optimum fit to the WA70 prompt photon data. It is therefore not surprising that the gluons from the various sets of partons are quite similar above $x \sim 10^{-2}$. Clearly, this does not reflect the true ambiguity in the gluon distribution, but rather it is an artifact of our economical parametrization. We will attempt to address this problem in a future publication. We will also evolve our distributions to lower Q^2, below Q_0^2=4 GeV^2, and study the interplay of leading and higher twists and, hence, provide a phenomenological representation of F_2 at low Q^2.

For the future we foresee a continued improvement in our knowledge of the partons. The increasingly precise measurements of F_2 at HERA, particularly at low x and low Q^2 ($Q^2 \sim 5$ GeV^2), may help to distinguish between BFKL and GLAP dynamics and may even reveal the onset of shadowing behavior. So far, the Drell-Yan asymmetry has only been measured at x=0.18. This leaves considerable ambiguity in the structure of $\bar{d} - \bar{u}$. The results of the asymmetry measurement by a forthcoming experiment at Fermilab [54] will cover an extended x interval and are eagerly awaited. The accuracy of the $W^{\pm}$ rapidity asymmetry measurements at Fermilab will improve and thus provide extremely tight constraints on the behavior of d/u in the x region around 0.05. The neutrino measurements at low x are under further study by the CCFR collaboration, and the discrepancy with the NMC measurements may be resolved. A change may effect the relative normalization between the data sets—an improvement here would be of great value. Finally, detailed studies of J/ψ $c\bar{c}$, $b\bar{b}$, prompt photon, and jet production at Fermilab and HERA, together with measurements of the longitudinal structure function F_L, will help reduce the ambiguity in the gluon distribution.

ACKNOWLEDGMENTS

We are grateful to Hiro Aihara, Bill Badgett, Arie Bodek, Antje Bruell, Robin Devenish, Albert De Roeck, Marcel Demarteau, Mark Dickson, Kevin Einsweiler, Henry Frisch, Walter Giele, Nigel Glover, Louis Kluberg, Sacha Kopp, Steven Kuhlmann, Michelangelo Mangano, Jeff Owens, Ewa Rondio, and Paul Slattery for useful discussions.

[1] H1 Collaboration, I. Abt *et al.*, Nucl. Phys. **B407**, 515 (1993); ZEUS Collaboration, M. Derrick *et al.*, Phys. Lett. B **316**, 412 (1993).

[2] H1 Collaboration, K. Müller, in Proceedings of the 29th Rencontre de Moriond, 1994 (unpublished).

[3] ZEUS Collaboration, G. Wolf, in Proceedings of the International Workshop on Deep-Inelastic Scattering, Eilat, Israel, 1994 (unpublished); M. Roco, in Proceedings of the 29th Rencontre de Moriond [2].

[4] NA51 Collaboration, A. Baldit *et al.*, Phys. Lett. B **332**, 244 (1994).

[5] CDF Collaboration, A. Bodek, in Proceedings of the International Workshop on Deep-Inelastic Scattering [3].

[6] NMC, P. Amaudruz *et al.*, Phys. Lett. B **295**, 159 (1992).

[7] BCDMS Collaboration, A. C. Benvenuti *et al.*, Phys. Lett. B **223**, 485 (1989).

[8] A. D. Martin, R. G. Roberts, and W. J. Stirling, Phys. Lett. B **306**, 145 (1993).

[9] E. A. Kuraev, L. N. Lipatov, and V. S. Fadin, Sov. Phys. JETP **45**, 199 (1977); Ya. Ya. Balitsky and L. N. Lipatov, Sov. J. Nucl. Phys. **28**, 822 (1978).

[10] A. D. Martin, R. G. Roberts, and W. J. Stirling, in *Proceedings of the Workshop on Quantum Field Theoretical Aspects of HE Physics*, Kyffhässer, Germany, 1993, edited by G. Geyer and E.-M. Ilgenfritz (University of Leipzig, Leipzig, 1993), p. 11.

[11] CTEQ Collaboration, J. Botts *et al.*, Phys. Lett. B **304**, 159 (1993), now superseded by CTEQ2, J. Botts *et al.* (unpublished).

[12] S. D. Ellis and W. J. Stirling, Phys. Lett. B **256**, 258 (1991).

[13] NMC, P. Amaudruz *et al.*, Phys. Rev. Lett. **66**, 2712 (1991).

[14] CCFR Collaboration, A. Bazarko *et al.*, Columbia University Report No. NEVIS-1492, 1993 (unpublished).

[15] M. A. G. Aivazis, F. I. Olness, and W.-K. Tung, Phys. Rev. D **50**, 3085 (1994); M. A. G. Aivazis, J. C. Collins, F. I. Olness, and W.-K. Tung, *ibid.* **50**, 3102 (1994).

[16] M. Glück, E. Reya, and M. Stratmann, Nucl. Phys. **B422**, 37 (1994).

[17] J. J. Aubert *et al.*, Nucl. Phys. **B213**, 31 (1983).

[18] S. J. Brodsky, P. Hoyer, C. Peterson, and N. Sakai, Phys. Lett. **93B**, 451 (1980).

[19] V. Barone *et al.*, Phys. Lett. B **268**, 279 (1991).

[20] A. D. Martin, R. G. Roberts, and W. J. Stirling, Phys. Rev. D **47**, 867 (1993).

[21] NMC, P. Amaudruz *et al.*, Report No. CERN-PPE/94-32, 1994 (unpublished).
[22] CCFR Collaboration, P. Z. Quintas *et al.*, Phys. Rev. Lett. **71**, 1307 (1993).
[23] B. Badelek and J. Kwieciński, Phys. Rev. D **50**, 4 (1994).
[24] WA70 Collaboration, M. Bonesini *et al.*, Z. Phys. C **38**, 371 (1988).
[25] E605 Collaboration, C. N. Brown *et al.*, Phys. Rev. Lett. **63**, 2637 (1989).
[26] G. Marchesini, in *Proceedings of the Workshop "QCD at 200 TeV,"* Erice, 1990, edited by L. Cifarelli and Yu. L. Dokshitzer (Plenum, New York, 1992), p. 183; S. Catani, F. Fiorani, and G. Marchesini, Phys. Lett. B **234**, 339 (1990); Nucl. Phys. **B336**, 18 (1990); S. Catani *et al.*, *ibid.* **B361**, 645 (1991).
[27] A. J. Askew, J. Kwieciński, A. D. Martin, and P. J. Sutton, Phys. Rev. D **47**, 3775 (1993); Mod. Phys. Lett. A **8**, 3813 (1993); Phys. Rev. D **49**, 4402 (1994).
[28] J. Kwieciński, in *Proceedings of the XXXII Internationale Universitätswochen für Kern- und Teilchenphysik*, Schladming, Austria, 1993, edited by L. Mathelitsch and W. Plessas (Springer-Verlag, Berlin, 1994), p. 215.
[29] M. Glück, E. Reya, and A. Vogt, Z. Phys. C **53**, 127 (1992); Phys. Lett. B **306**, 391 (1993).
[30] A. Capella, A. Kaidalov, C. Merino, and J. Tran Thanh Van, Orsay Report No. LPTHE-93-34, 1994 (unpublished).
[31] A. J. Askew *et al.*, Phys. Lett. B **325**, 212 (1994).
[32] R. K. Ellis, Z. Kunszt, and E. M. Levin, Nucl. Phys. **B420**, 517 (1994).
[33] A. D. Martin, R. G. Roberts, and W. J. Stirling, Phys. Rev. D **37**, 1161 (1988).
[34] W. T. Giele, E. W. N. Glover, and D. Kosower, Nucl. Phys. **B403**, 633 (1993).
[35] A. D. Martin, R. G. Roberts, and W. J. Stirling, Mod. Phys. Lett. A **4**, 1135 (1989); E. L. Berger, F. Halzen, C. S. Kim, and S. Willenbrock, Phys. Rev. D **40**, 83 (1989).
[36] A. D. Martin and W. J. Stirling, Phys. Lett. B **237**, 551 (1990).
[37] UA6 Collaboration, G. Sozzi *et al.*, Phys. Lett. B **317**, 243 (1993).
[38] A. D. Martin, R. G. Roberts, and W. J. Stirling, Phys. Lett. B **266**, 173 (1991); Phys. Rev. D **43**, 3648 (1991).
[39] A. M. Cooper-Sarkar *et al.*, Z. Phys. C **39**, 281 (1988).
[40] H1 Collaboration, I. Abt *et al.*, Phys. Lett. B **321**, 161 (1994).
[41] CDF Collaboration, F. Abe *et al.*, in *Lepton and Photon Interactions*, Proceedings of the 16th International Conference, Ithaca, New York, 1993, edited by P. Drell and D. Rubin, AIP Conf. Proc. No. 302 (AIP, New York, 1994).
[42] A. D. Martin, R. G. Roberts, and W. J. Stirling, Phys. Lett. B **318**, 184 (1993).
[43] CDF Collaboration, F. Abe *et al.*, Phys. Rev. Lett. **68**, 2734 (1992); Phys. Rev. D **48**, 2998 (1993); in *Lepton and Photon Interactions* [41].
[44] M. Glück, L. E. Gordon, E. Reya, and W. Vogelsang, Phys. Rev. Lett. **73**, 388 (1994).
[45] J. E. Huth and M. L. Mangano, Annu. Rev. Nucl. Part. Sci. **43**, 585 (1993).
[46] D0 (presented by E. James) and CDF (presented by M. Franklin) Collaborations, International Symposium on "Physics Doesn't Stop: Recent Developments in Phenomenology," Madison, Wisconsin, 1994 (unpublished).
[47] R. Hamberg, T. Matsuura, and W. L. van Neerven, Nucl. Phys. **B345**, 331 (1990); **B359**, 343 (1991); W. L. van Neerven and E. B. Zijlstra, *ibid.* **B382**, 11 (1992).
[48] CDF Collaboration, F. Abe *et al.*, Phys. Rev. Lett. **69**, 28 (1992).
[49] D0 Collaboration, P. Grudberg and C. Gerber, Bull. Am. Phys. Soc. **39**, 1236 (1994).
[50] CDF Collaboration, F. Abe *et al.*, Phys. Rev. D **50**, 5550 (1994).
[51] CDF Collaboration, F. Abe *et al.*, Phys. Rev. D **50**, 2966 (1994).
[52] P. Nason, S. Dawson, and R. K. Ellis, Nucl. Phys. **B312**, 607 (1989); W. Beenakker, H. Kuijf, W. L. van Neerven, and J. Smith, Phys. Rev. D **40**, 54 (1989).
[53] E. Laenen, J. Smith, and W. L. van Neerven, Nucl. Phys. **B369**, 543 (1992); Phys. Lett. B **321**, 254 (1994).
[54] G. T. Garvey *et al.*, Fermilab proposal No. P866, 1992 (unpublished).

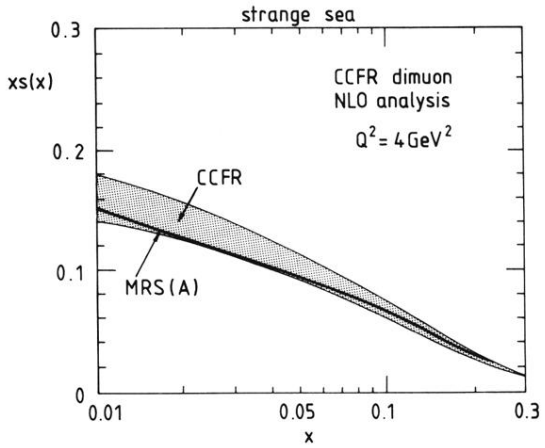

FIG. 4. The shaded band is the strange sea quark distribution xs (x, Q^2=4 GeV^2), determined by the CCFR Collaboration [14] from a next-to-leading-order analysis of their dimuon production data. In addition, they find that $s/(\bar{u}+\bar{d})$ is, to a good approximation, independent of x. Also shown is the MRS(A) input strange sea quark distribution xs ($x, Q_0^2 = 4$ GeV^2), as given in Eq. (7).